NASA TECHNICAL MEMORANDUM

NASA TM X-3049

NASA TM X-3049

FLIGHT VELOCITY EFFECTS ON THE JET NOISE OF SEVERAL VARIATIONS OF A 104-TUBE SUPPRESSOR NOZZLE

by Richard R. Burley

Lewis Research Center
Cleveland, Ohio 44135

NATIONAL AERONAUTICS AND SPACE ADMINISTRATION • WASHINGTON, D. C. • JULY 1974

1. Report No.	2. Government Accession No.	3. Recipient's Catalog No.
NASA TM X-3049		

4. Title and Subtitle	5. Report Date
FLIGHT VELOCITY EFFECTS ON THE JET NOISE OF SEVERAL VARIATIONS OF A 104-TUBE SUPPRESSOR NOZZLE	JULY 1974
	6. Performing Organization Code
7. Author(s)	8. Performing Organization Report No.
Richard R. Burley	E-7901
	10. Work Unit No.
9. Performing Organization Name and Address	501-24
Lewis Research Center National Aeronautics and Space Administration Cleveland, Ohio 44135	11. Contract or Grant No.
	13. Type of Report and Period Covered
12. Sponsoring Agency Name and Address	Technical Memorandum
National Aeronautics and Space Administration Washington, D.C. 20546	14. Sponsoring Agency Code

15. Supplementary Notes

16. Abstract

At the relatively high takeoff speeds of supersonic transport aircraft, an important question concerns whether the flight speed affects the noise of suppressor nozzles. To answer this question, flyover and static tests using a modified F-106B aircraft were conducted on a 104-tube suppressor nozzle. Comparison of adjusted flyover and static spectra indicated that flight velocity had a small adverse effect on the suppression of the 104-tube suppressor. The adverse effect was larger with the acoustic shroud installed than without it.

17. Key Words (Suggested by Author(s))	18. Distribution Statement
Flight velocity effect; Jet noise suppressors; Nozzle thrust; Propulsion systems; Ejector nozzle	Unclassified - unlimited Category 28

19. Security Classif. (of this report)	20. Security Classif. (of this page)	21. No. of Pages	22. Price*
Unclassified	Unclassified	51	$3.75

* For sale by the National Technical Information Service, Springfield, Virginia 22151

FLIGHT VELOCITY EFFECTS ON THE JET NOISE OF SEVERAL VARIATIONS OF A 104-TUBE SUPPRESSOR NOZZLE

by Richard R. Burley

Lewis Research Center

SUMMARY

At the relatively high takeoff speeds of supersonic transport aircraft, an important question concerns whether the flight speed affects the noise of suppressor nozzles. To answer this question, flyover and static tests were conducted on a 104-tube suppressor nozzle. The effects of incorporating an acoustical shroud and scoops also were studied. The tests were conducted by using an F-106B aircraft modified to carry two underwing nacelles, each containing a calibrated J85-GE-13 turbojet engine. Data were taken over a range of J85 engine power settings that resulted in relative jet velocities from 418 to 625 meters per second (1370 to 2050 ft/sec) for static conditions and from 381 to 537 meters per second (1250 to 1760 ft/sec) for flyover conditions.

Comparison of the adjusted flyover and static spectra at the acoustic angle that resulted in peak flyover noise indicated that flight velocity had a small adverse effect on the suppression of the 104-tube suppressor. Installing the acoustic shroud slightly increased the adverse effect. The frequency spectrum for the 104-tube suppressor in flyover contains only a small amount of low-frequency and midfrequency noise but about as much high-frequency noise as the baseline nozzle. The high-frequency noise peaked at a frequency of 3200 hertz. Installing the acoustical shroud attenuated the noise by as much as 12.5 dB at a frequency of 3200 hertz. When the acoustic data from the flyover tests were scaled up from J85 engine size (0.23 scale) to full scale and then extrapolated to a sideline distance of 648 meters (2128 ft) from an altitude of 305 meters (1000 ft), the 104-tube suppressor with an acoustic shroud reduced the peak noise level by 14.5 EPNdB (relative to the baseline nozzle). This reduction was achieved with a thrust penalty of 14.3 percent, which made it the most effective of the 104-tube suppressor configurations tested.

INTRODUCTION

During takeoff of supersonic transport aircraft, the dominant noise source is the high-velocity jet issuing from the exhaust nozzle. Acoustic characteristics of both unsuppressed and suppressor exhaust nozzles have generally been investigated at static conditions (cf. refs. 1 to 3). However, the takeoff speed of these aircraft can be as high as Mach 0.35 when maximum sideline noise is recorded. Thus, an important question concerns whether flight speed affects the noise of exhaust nozzles.

To gain some insight into this question, flyover and static tests are being conducted on both unsuppressed and suppressor exhaust nozzles. Some preliminary results were published in references 4 and 5. The investigation of three basic types of unsuppressed nozzles reported in reference 6 showed that flight speed has a beneficial effect on the noise of an auxiliary inlet ejector nozzle. Results for a wide variety of suppressor configurations (refs. 7 to 9) showed no beneficial effect on the noise of suppressors installed on a plug nozzle (there was either no effect or an adverse effect). However, since the noise of a basic unsuppressed auxiliary inlet ejector nozzle benefited from flight speed, the installation of a suppressor on this nozzle might also result in a favorable effect.

The present investigation was conducted to determine whether flight speed affects the noise and thrust of a 104-elliptical tube suppressor installed on an auxiliary inlet ejector nozzle. The configuration is based on the design described in reference 10. The suppressor was tested with no shroud and with an acoustically lined shroud. The effect of scoops also was studied.

The tests were conducted by using an F-106B aircraft modified to carry podded engines mounted near the aft lower surface of the wing with the exhaust nozzles extending beyond the wing trailing edge. The primary jet exhaust was provided by calibrated J85-GE-13 turbojet engines. The flyovers were conducted at an altitude of 91 meters (300 ft) and a Mach number of 0.4. Acoustic measurements were taken from a ground station directly beneath the flight path. For static tests, the acoustic measurements were taken at a radial distance of 30.48 meters (100 ft) from the nozzle. Data were taken over a range of J85 engine power settings from part throttle to military power. This gives a range of relative jet velocities from 418 to 625 meters per second (1370 to 2050 ft/sec) for static conditions and from 381 to 536 meters per second (1250 to 1760 ft/sec) for flyover conditions.

SYMBOLS

A_8 primary nozzle exit effective flow area (hot), cm^2; sq in.

D nozzle drag, kN; lbf

D_{BP}	baseplate pressure drag, kN; lbf
d	diameter, cm; in.
d_n	nacelle diameter, 63.5 cm (25 in.)
EPNL	effective perceived noise level, EPNdB
F	thrust, kN; lbf
$F_{i,p}$	ideal thrust of primary jet, kN; lbf
H	aircraft altitude, m; ft
h_m	height of microphone above concrete surface, m; ft
M_O	flight Mach number
OASPL	overall sound pressure level, dB (referenced to 2×10^{-5} N/m^2
PNL	perceived noise level, PNdB
P_8	total pressure at primary nozzle exit, kN/m^2; psia
P_8/p_0	nozzle pressure ratio
p_{BP}	static pressure on baseplate, kN/m^2; psia
p_0	ambient static pressure, kN/m^2; psia
R_p	direct ray distance between exhaust nozzle and microphone (see fig. 13(c)), m; ft
$R_{p,a}$	adjusted direct ray distance (see fig. 13(c)), m; ft
r	radius, cm; in.
r_β	boattail juncture radius, cm; in.
T_g	total temperature at primary nozzle exit, K; ^oR
T_s	total temperature of secondary air, K; ^oR
V_a	aircraft velocity, m/sec; ft/sec
V_j	ideal jet velocity, m/sec; ft/sec
V_R	relative jet velocity, $V_j - V_a$, m/sec; ft/sec
W_s	secondary weight flow, kg/sec; lbm/sec
W_8	weight flow at primary nozzle exit, kg/sec; lbm/sec
$(WL)_s$	image length of wing, cm; in.
X	linear measurement (see fig. 13(d)), cm; in.
Y	lateral displacement of aircraft (see fig. 13(c)), m; ft

Y_m image length of lateral displacement (see fig. 13(d)), cm; in.

θ angle between direct ray and jet centerline, deg

$\omega\sqrt{\tau}$ corrected secondary weight flow ratio, $\frac{W_s}{W_8}\sqrt{\frac{T_s}{T_8}}$

APPARATUS AND PROCEDURE

Test Facility

Flyover and static tests were conducted with an F-106B aircraft modified to carry two underwing nacelles. The aircraft is shown in flight in figure 1. A schematic view of the nacelle-engine installation is shown in figure 2. The 63.5-centimeter- (25.0-in.-) diameter nacelles were located at approximately 32 percent semispan with the exhaust nozzles extending beyond the wing trailing edge. Since the nozzle would interfere with normal elevon movement, a section of the elevon immediately above each nacelle was cut out and rigidly fixed to the wing. Each nacelle contained a calibrated J85-GE-13 afterburning turbojet engine. The nacelles had normal shock inlets with blunted cowl lips for the flyover tests. Secondary air to cool the engine and afterburner was supplied from the inlet and was controlled at the periphery of the compressor face by a calibrated rotary valve. For the static tests, the blunted cowl lips were replaced with a bellmouth as shown in figure 3.

Each nacelle was attached to the wing by two links normal to the nacelle axis, and the axial force was measured by a load cell attached to the wing as shown in figure 2. An accelerometer in the nacelle allowed the load cell to be compensated for acceleration. The axial force transmitted to the compensated load cell can be divided into two parts: (1) nacelle drag forward of the research nozzle, referred to as the tare force; and (2) research nozzle gross thrust minus drag. Gross thrust minus drag was determined by adding the tare force to the compensated load cell reading. The tare force was zero for static tests (ref. 6). For flyover tests, the tare force was the sum of the ram drag and the skin friction drag on the nacelle and strut (ref. 6).

Baseline Nozzle

The baseline nozzle used for this study was the unsuppressed plug nozzle shown in figure 4. It consisted of a 10° half-angle conical plug body and a primary flap with a 14° trailing edge. A plug nozzle generally has a translating outer shroud, which is retracted for efficient operation at the low pressure ratios for takeoff conditions. The present

configuration simulates the shroud in this position. Further details of this nozzle design are given in reference 11; acoustic and thrust results for flyover conditions are presented in reference 6.

Suppressor Configurations

The suppressor configurations are shown in figure 5. The 104-tube nozzle installed on the aircraft is shown in figure 5(a); details of the nozzle are shown in figures 5(b) and (c). The tubes, which have an elliptical shape, are mounted on a conical baseplate with the tube major axis in the radial direction. The ratio of the area circumscribing the mixing nozzle to the primary effective area is 2.8. The tubes are divided into five rows. All the tubes in a given row have the same length. The tubes in the outer row are the longest, 9.22 centimeters (3.63 in.) long, and the ventilation factor (ratio of side flow area between outer row of tubes to base area) is about 0.6. Conceptually, the array of tubes would be divided into four segments, and for unsuppressed operation these segments would be retracted into the space around the primary nozzle, where they would be completely out of the exhaust gas stream (fig. 5(d)).

The acoustic shroud installed on the suppressor is shown in figure 5(e), and details of the shroud are given in figure 5(f). The acoustic shroud had a maximum cavity depth of 4.57 centimeters (1.81 in.) resulting in a shroud exit diameter of 53.80 centimeters (21.18 in.). The outer surface of the shroud had a boattail angle of 10° and a boattail juncture radius of 0.5 nacelle diameter. The acoustic treatment consisted of a perforated plate adjacent to the hot jet, a bulk absorber, and a solid backing plate. Baffle disks, used for structural integrity, also prevented axial movement of the bulk absorber and served as resonator walls. The stainless-steel perforated plate was 0.079 centimeter (0.031 in.) thick and had 0.198-centimeter- (0.078-in.-) diameter holes and a 23 percent open area. The bulk absorber was 0.028-centimeter- (0.011-in.-) diameter stainless-steel wire mesh that filled each cavity to a density of 322 kilograms per cubic meter (20 lb/ft^3). Because the absorber is of the bulk type and because it is exposed to high gas flow velocities and sound pressure levels, the liner probably will act as a broad band absorber (ref. 12).

The scoops installed on the suppressor with the acoustic shroud are shown in figure 5(g); details of the scoops are given in figures 5(h) and (i). The scoops, which were 33 centimeters (13 in.) long, were at an angle of about 22°, and the downstream ends of the scoops were in the same plane as the tubes.

Instrumentation

An onboard digital data system was used to record pressures, temperatures, and load cell output on magnetic tape. It had the capability of recording 578 parameters in 11.5 seconds (ref. 13). A flight calibrated test boom located on the aircraft nose was used to determine free-stream static and total pressure, aircraft angle of attack, and yaw angle. Aircraft speed was obtained from a calibrated machmeter, the output of which was sampled and recorded six times in 11.5 seconds by an onboard digital data system.

Aircraft altitude and position were determined with the aid of the Polaroid Land camera shown in figure 6(a). The camera, located near the microphone, was used to take a picture of the aircraft as it flew over the microphone. A typical picture is shown in figure 6(b). Further details are given in appendix A.

Engine airflow was determined by using the calibration results from reference 14 along with measurements of engine speed and total pressure and temperature at the compressor face. Fuel flows were obtained from calibrated flowmeters. Temperature T_8, total pressure P_8, and effective area A_8 were obtained by using the values of engine airflow and fuel flow, the measured values of total pressure and temperature at the turbine discharge, and afterburner temperature rise and pressure drop calibration results from reference 14. Calibrations of the secondary flow valve pressure drop and position were used to determine secondary airflow.

Total pressures and temperatures of the secondary air were obtained from probes, as shown in figure 7. Static-pressure orifices on the baseplate of the primary nozzle are shown in figure 8.

The noise measuring instrumentation is shown in the block diagram of figure 9. The microphone was ceramic and 2.54 centimeters (1 in.) in diameter and had a frequency response that was flat to within ±2 dB for grazing incidence over the frequency range used. The output of the microphone was recorded on a two-channel direct-recording tape recorder. The entire system was calibrated for sound level in the field before and after each test with a conventional tone calibrator. The tape recorder was calibrated for linearity with a "pink" noise generator (constant energy per octave).

The flyover signal, recorded on magnetic tape, was played back through 1/3-octave band filters and then reduced to a digital form (see fig. 9(b)). The averaging time used for data reduction was 0.1 second. The digital results were recorded on a tape. The time history of each flyover (in terms of PNL) and three associated frequency spectra (at peak PNL and 10 PNdB down on either side) were automatically plotted.

The static signal recorded on magnetic tape was played back through 1/3-octave band filters, and the spectra were automatically plotted (see fig. 9(c)). The averaging time used during data reduction was 1/8 second. The plotted results were converted into digital form and recorded on tape.

Meteorological conditions, in terms of dry-bulb and dew-point temperatures, wind speed and direction, and barometric pressure, were recorded periodically throughout the test. Wing speeds were less than 5.144 meters per second (10 knots) during the tests.

Procedure

The microphone stations for the acoustic measurements are shown in figure 10 for static conditions. The portable microphone was positioned 1.22 meters (4 ft) above the concrete surface and was oriented to receive the acoustic pressure wave at normal incidence (see fig. 10(a)). The microphone was fitted with a wind screen that caused no loss of signal. The acoustic measurements were made at a radial distance of 30.48 meters (100 ft) from the nozzle exit in increments of 10° over a 90° sector (see fig. 10(b)). During the measurements, the main J75 engine was at idle power. The J85 engine in the nacelle containing the research nozzle was operated over a range of power settings, and the J85 engine in the other nacelle was shut off.

Background noise levels for the static tests were determined with both J85 engines shut off, the J75 engine at idle power, and external cooling air on. It was necessary to supply air from an external source to cool the J85 engine when it was operating at the military power setting. The air was supplied from an air start cart which was located on the far side of the aircraft (see fig. 11). The supply line went from the start cart to the J85 engine, and the air was directed around the engine through a nozzle (see fig. 3). The J75 engine had to be operating when static data were taken because it supplied the electrical power for the onboard digital data system.

The frequency spectra for the background noise (with the J75 engine at idle power and external cooling air on) and for the suppressor configurations are compared in figure 12 at an acoustic angle of 70°. (An acoustic angle of 70°, as subsequently shown in the section Acoustic Characteristics, is about where the suppressor configurations reach their peak noise level.) Background noise level generally tends to increase as the frequency increases, from a level of 74 dB at a frequency of 100 hertz to a level of 83 dB at a frequency of 5000 hertz. The shaded region represents sound pressure levels that are 10 dB or less above the background noise level. Background noise does not significantly influence noise of the suppressor configurations as long as the spectra of these configurations remain above the shaded region. The spectrum for the bare suppressor generally is above the shaded area. This is not the case for the suppressor with the acoustic shroud, however, where the sound pressure level values between frequencies of 1250 and 4000 hertz are well within the shaded region. However, the influence is small, and after the influence of the background noise is removed, the perceived noise level of this

configuration is reduced less than 0.5 PNdB. Thus, the background noise does not significantly interfere with the peak noise of the suppressor configurations.

Acoustic measurements of the flyover noise were made from a ground station under the flight path. The microphone setup is shown in figure 13(a). The microphone was positioned 1.22 meters (4 ft) above the concrete surface. It was fitted with a wind screen that caused no loss of signal and was oriented to receive the acoustic pressure waves at grazing incidence.

As the aircraft travels along its flight path, the direct ray distance from the nozzle to the microphone R_p continuously changes (see fig. 13(b)). The angle between the direct ray and the jet centerline, referred to as the acoustic angle θ, also changes. The relation between R_p and θ shown in figure 13(b) assumes the aircraft flys directly over the microphone at an altitude of exactly 91 meters (300 ft). (See ref. 6 for the discussion concerning the selection of this altitude.) But since this may not always be the case, provisions were made to adjust the recorded sound pressure level to these conditions. Details are given in appendix A.

While the noise data were being recorded during the flyovers, the main engine of the aircraft was at idle power. The J85 engine in the nacelle that contained the research nozzle was operated at military and part power settings. The J85 engine in the opposite nacelle was shut off and allowed to windmill.

Background noise level during flyover was determined with the main engine at idle power and both J85 engines shut off and allowed to windmill. The results are shown in figure 14 adjusted to standard day and free-field conditions. Figure 14(a) presents the variation of background perceived noise level with acoustic angle. At an acoustic angle of 40° (peak noise level for the baseline nozzle and where one comparison of frequency spectra was made), the background noise level was about 91 PNdB. At an acoustic angle of 70° (peak noise level for suppressor configurations), the background noise level was about 96 PNdB. Figure 14(b) presents the frequency spectrum associated with the acoustic angle of 40°. The spectrum was fairly constant at a level of 67 dB between frequencies of 125 and 3200 hertz; it decreased to a level of about 62 dB at a frequency of 6300 hertz. Figure 14(c) presents the frequency spectrum associated with the acoustic angle of 70°. It was adjusted to a distance of 30.48 meters (100 ft) from the noise source (distance at which another comparison of frequency spectra was made). The spectrum was fairly constant at a level of about 82 dB between frequencies of 125 and 5000 hertz; it decreased to a level of 77 dB at a frequency of 8000 hertz. Both of the background noise levels were sufficiently low so they did not markedly interfere with noise from the suppressor nozzle.

RESULTS AND DISCUSSION

Acoustic Characteristics

To investigate whether flight velocity affects the noise of the 104-tube suppressor configurations, the approach was to adjust the measured flyover and static spectra to comparable conditions of 30.48 meters (100 ft) from the nozzle in the free field and on a standard day. The Doppler shift of frequency, which was accounted for in the flyover spectra, caused a maximum shift of frequency of one 1/3-octave band. Details of the adjustments are given in reference 6. The adjusted flyover and static spectra then were compared at a constant relative jet velocity of 536 meters per second (1760 ft/sec) and for the acoustic angle that resulted in peak flyover noise. Significant differences between these adjusted spectra would be attributed to flight velocity.

In making the comparison, the greatest emphasis should be placed on the data at frequencies between 160 and 5000 hertz. At frequencies below 160 hertz, the short integration time, the narrowness of the frequency bands, and the rapidly changing conditions of the flyover combine to give results that are less reliable. At frequencies above 5000 hertz, the acoustic signal received at the ground station quite possibly is below the noise floor of the recording equipment (ref. 15). Values of the atmospheric absorption coefficient are very large at these high frequencies and multiply the noise floor to unrealistically high noise levels when the data are adjusted to 30.48 meters (100 ft).

A comparison of the flyover and static spectra for the 104-tube suppressor nozzle is shown in figure 15. The flyover spectrum is very close to the static spectrum from 160 to 630 hertz but considerably above the static spectrum at higher frequencies. This difference results in OASPL and PNL values that were about 2 dB higher for the flyover than for the static spectrum. It suggests that flight velocity had a small adverse effect on suppression.

A comparison of the flyover and static spectra for the 104-tube suppressor with an acoustic shroud is shown in figure 16. The flyover spectrum is slightly higher than the static spectrum from 160 to 630 hertz and considerably above it at the higher frequencies. This difference results in an OASPL value 2 dB higher and a PNL value 3 PNdB higher for the flyover than for the static spectrum. It suggests that flight velocity also had an adverse effect on the suppressor with an acoustic shroud. The adverse effect seems to be slightly greater with the acoustic shroud than without it.

In an attempt to increase suppression and to reduce the drag on the conical baseplate, scoops were installed on the 104-tube suppressor with an acoustic shroud. A comparison of the flyover and static spectra for this configuration is shown in figure 17. Again the flyover spectrum is above the static spectrum and results in an OASPL value 2 dB higher and a PNL value 3 dB higher for the flyover spectrum. Thus, the scoops

were not effective in reducing the adverse effect of flight velocity. Consequently, no further noise results will be presented for them.

The comparisons just presented were based on using relative jet velocity as the primary static-to-flyover correlating parameter principally because it gives reasonably valid results when applied to conical nozzles (ref. 16). But jet noise radiated from a suppressor nozzle has a spectrum different from that of noise radiated from a conical nozzle and, therefore, might respond differently to airplane velocity. The spectrum of a suppressor nozzle has a high-frequency portion generated close to the nozzle exit plane by the mixing of the elemental jets with the ambient air and a low-frequency portion generated farther downstream after the elemental jets and the entrained air have merged into a single large jet. A correlating parameter for use with ejector-suppressor nozzles was suggested in reference 16. Noise generated aft of an ejector shroud (i.e., low-frequency noise) is correlated with relative jet velocity; noise generated within an ejector shroud (i.e., high-frequency noise) is correlated with elemental jet velocity minus shroud secondary air velocity.

A preliminary indication of the validity of this correlating parameter can be obtained by examining the spectra shown in figures 15 and 16. They tend to confirm that relative jet velocity might be a proper correlating parameter for the low-frequency noise since reasonably good agreement is obtained at frequencies between 160 and 630 hertz. However, the high-frequency portion of the 104-tube suppressor without an acoustic shroud (fig. 15) also appears to correlate with relative jet velocity since the peak value for the flyover spectrum is only slightly higher (about 1.5 dB) than that of the static spectrum. When the acoustic shroud is installed on the 104-tube suppressor (fig. 16), the high-frequency portion appears to correlate with a velocity between jet velocity and relative jet velocity, as suggested in reference 16. Noise levels for the high frequencies were 3 to 4 dB higher in flyover than for static conditions. The remaining comparisons will be made on the basis of relative jet velocity.

Another indication of flight velocity effect is directivity and peak noise level. In figure 18 the variation in perceived noise level with acoustic angle during a typical flyover at an altitude of 91 meters is compared to that predicted from data extrapolated to a 91-meter sideline. Figure 18(a) shows the results for the 104-tube suppressor nozzle. The flyover noise level reached a peak value of about 111 PNdB at an angle of about 70°. Static results predicted a somewhat lower peak value (109.5 PNdB) occurring about 10° closer to the jet axis. Figure 18(b) shows the results for the 104-tube suppressor with an acoustic shroud. The flyover noise level reached a peak value of about 108 PNdB at an angle of about 70°. Again the static results predicted a lower peak value (104 PNdB) occurring slightly (about 5°) farther away from the jet axis.

The results of the flyover tests for two of the suppressor configurations are shown in figure 19 in terms of the variation in perceived noise level with acoustic angle. For comparison, the results for the unsuppressed plug nozzle, used as the baseline nozzle,

also are shown. The results are presented at a relative jet velocity of 536 meters per second (1760 ft/sec). The background noise level, discussed in the section APPARATUS and PROCEDURE, is also shown.

The baseline nozzle had a peak noise level of 117 PNdB occurring at an acoustic angle of 40°. Peak noise level of the 104-tube suppressor was about 6 PNdB below that of the baseline nozzle and occurred about 20° farther away from the jet axis. Installing the acoustic shroud resulted in a further reduction of 2.5 PNdB in peak noise level and shifted it about 7° farther away from the jet axis when compared with the suppressor without the shroud.

The flyover results just discussed were for a constant relative jet velocity. The effect on peak flyover noise level of decreasing the relative jet velocity is shown in figure 20. If the results for a particular suppressor configuration are compared to those for the baseline nozzle, the effectiveness of that particular suppressor as a function of relative jet velocity can be determined. Reducing the relative jet velocity adversely affected the suppression of the 104-tube suppressor. The suppression is only 3 PNdB at a relative jet velocity of 460 meters per second (1500 ft/sec) compared to 6 PNdB at a relative jet velocity of 537 meters per second (1760 ft/sec). Although there was an increase in suppression when the acoustic shroud was installed, the trend of reduced effectiveness with decreasing relative jet velocity was not significantly altered. The suppression was 5.5 PNdB at a relative jet velocity of 460 meters per second (1500 ft/sec) compared to 8.5 PNdB at a relative jet velocity of 537 meters per second (1760 ft/sec). Even at the lowest relative jet velocity shown, peak background noise (99 PNdB; fig. 19) does not markedly interfere with the noise of the research nozzles.

For all of the configurations, a noise floor was being reached. This noise floor, which was different from the one mentioned in the section APPARATUS AND PROCEDURE, is probably the result of internally generated noise from the J85 engine. This noise was considered to be associated with the highly turbulent flow inside the engine tailpipe and exhaust nozzle (ref. 17), which will dominate at low jet velocities. Conventional noise suppressors appear to be ineffective in suppressing internally generated noise.

The flyover spectra for the 104-tube suppressor with and without its acoustic shroud are shown in figure 21 along with the spectrum for the baseline nozzle. The results are presented for a relative jet velocity of 502 meters per second (1660 ft/sec) and at the acoustic angle that resulted in peak flyover noise for the baseline nozzle (i.e., $\theta = 40^{\circ}$). Compared to the baseline nozzle, the 104-tube suppressor contains only a small amount of noise in the frequencies between 630 and 1250 hertz. This suggests that a considerable amount of external air was entrained in the large single jet and thereby reduced its velocity substantially. At the high frequencies, the amount of noise generated by the 104-tube suppressor approaches that for the baseline nozzle, which suggests that a substantial amount of mixing has occurred between the elemental jets and the surrounding

air. The high-frequency noise peaked at about 3200 hertz. Incorporating the acoustic shroud lowered the spectrum level at the high frequencies. The reduction amounted to 12 dB at a frequency of 3200 hertz. The acoustic shroud, as expected, acted as a broad band absorber because the absorption material was of the bulk type and because of the high sound pressure levels and high gas flow velocities to which the liner was exposed.

Thrust Characteristics

In addition to acoustic characteristics, thrust characteristics also are important. Thrust performance is presented in figure 22 in terms of nozzle gross thrust coefficient as a function of nozzle pressure ratio and relative jet velocity. To determine the thrust penalty, results for the baseline nozzle also are shown.

Thrust performance at static conditions is shown in figure 22(a). The baseline nozzle has a gross thrust coefficient of 0.99 at a nozzle pressure ratio of 2.1. Installing the 104-tube suppressor lowered the thrust coefficient to 0.90, which is a 9-percent reduction from the baseline nozzle at a pressure ratio of 2.1. One of the two factors contributing to this thrust loss is the drag caused by the base pressures being lower than ambient. This factor accounted for most of the loss, about 6 percent (the ratio of base pressure drag to ideal primary thrust was estimated to be 0.056, as shown in appendix B). The other factor is the increased wetted surface area (excluding base area) of the 104-tube suppressor over that of the baseline nozzle, which results in decreased internal thrust. This probably accounted for the remaining 3 percent of the thrust loss.

Installing the acoustic shroud raised the thrust coefficient to 0.915 and resulted in a 1.7-percent increase from the bare 104-tube suppressor at a pressure ratio of 2.1. This occurred even though the pressure drag on the baseplate almost doubled (the ratio of base drag to ideal primary thrust increased to 0.104 from 0.056, as shown in appendix B). Thus, the ejector pumped enough external air not only to overcome the increased pressure drag on the baseplate but also to achieve a 1.7-percent increase in gross thrust. For both suppressor configurations, thrust loss increased as nozzle pressure ratio decreased.

Thrust performance at flyover conditions is shown in figure 22(b). The baseline nozzle had a thrust coefficient of 0.965 at a pressure ratio of 2.4. Installing the 104-tube suppressor lowered the thrust coefficient to 0.827, which is a 14.3-percent reduction from the baseline nozzle at a pressure ratio of 2.4. Pressure drag on the baseplate accounted for most of the loss, about 10 percentage points (the ratio of base pressure drag to ideal primary thrust was estimated to be 0.098, as shown in appendix B). Internal flow losses probably accounted for the remaining 4 percentage points.

The thrust coefficient remained at 0.827 when the acoustic shroud was installed. Pressure drag on the baseplate decreased slightly (the ratio of base pressure drag to

ideal primary thrust decreased to 0.084, as shown in appendix B). Most of this decrease probably was counterbalanced by the external drag associated with the acoustic shroud. Also, there probably was no net thrust from the ejector because of the large ram drag associated with bringing the air onboard (ram drag was zero at static conditions).

Installing the scoops on the 104-tube suppressor with the acoustic shroud lowered the thrust coefficient to 0.735 and resulted in an 11-percent thrust loss from the configuration without the scoops at a nozzle pressure ratio of 2.4. The scoops were supposed to force external air into the base region and thereby reduce base drag substantially. This was not achieved since the base drag decreased only slightly (the ratio of base pressure drag to ideal primary thrust decreased to 0.079 from 0.084, as shown in appendix B). For this configuration as well as for the other two suppressor configurations, thrust loss relative to the baseline nozzle was not markedly affected by reducing nozzle pressure ratio.

Another important question concerns the effect of flight velocity on the thrust coefficient of the suppressor configurations. This can be seen in figure 23 by comparing the static and flyover results from figure 22. Figure 23(a) shows the comparison for the 104-tube suppressor without the acoustic shroud. Flight velocity had a large adverse effect on the thrust coefficient over the entire range of pressure ratios. At a pressure ratio of 2.3, the thrust coefficient decreased 8.2 percentage points; the adverse effect became even more pronounced as pressure ratio decreased. The adverse effect of flight velocity was largely due to the increased pressure drag on the baseplate (see appendix B), which indicated that the ventilation was much worse for flyover than for static conditions.

The effect of flight velocity on the suppressor with the acoustic shroud installed is shown in figure 23(b). Again flight velocity had a large adverse effect on the thrust coefficient over the entire range of pressure ratios. At a pressure ratio of 2.3, thrust coefficient decreased 10 percentage points; the adverse effect became somewhat more pronounced as pressure ratio decreased. However, ventilation was not the cause, since the effect of flight velocity was to decrease the ratio of baseplate pressure drag to ideal primary thrust. At a nozzle pressure ratio of 2.3, this ratio decreased from 0.104 to 0.086 (see appendix B). Thus, the gross thrust coefficient would have increased, had there been no other drag forces. However, there were two other sources of drag. One was a drag on the external surface of the acoustic shroud due to flight velocity. This drag force probably counterbalanced most of the decrease in baseplate pressure drag. The other source of drag was the ram drag associated with bringing the external air into the ejector at flyover conditions. This probably was the principal reason for the adverse effect of flight velocity on thrust coefficient.

Suppressor Effectiveness

The suppressor configurations tested were 0.23 scale (J85 engine size) models for a supersonic transport engine. To determine suppressor effectiveness, acoustic data from the flyover tests were scaled up to full size (four 267-kN- (60 000-lb-) thrust engines). This was done by using the Strouhal number relation (ref. 18) with the assumption that both the 0.23 scale and the full-scale engines were operating with identical primary gas conditions of pressure ratio, total temperature, and gas composition. It was further assumed that both the 0.23 scale and the full-scale suppressors were exposed to identical flight speeds and were influenced in an identical manner by flight speed.

After being adjusted to free-field conditions (ref. 6) and to standard day conditions (by the simplified procedure outlined in ref. 19), the full-scale acoustic results were extrapolated to a sideline distance of 648 meters (2128 ft) from an altitude of approximately 305 meters (1000 ft). This was done by accounting for inverse-square radiation and atmospheric absorption. Values of OASPL and PNL were obtained from the resulting spectrum at a particular instant of time.

The entire procedure then was repeated for a number of time points. Finally a time history, in terms of PNL, was constructed, and a value of EPNL was obtained (by the procedure outlined in ref. 19).

Suppressor effectiveness for two suppressor configurations (with and without an acoustic shroud) is presented in figure 24 in terms of EPNL suppression (EPNdB) as a function of percent thrust loss (relative to the baseline nozzle). The results are shown for a Mach number of 0.4 and a nozzle pressure ratio of 2.4 (relative jet velocity of 537 m/sec (1760 ft/sec)). The suppressor was more effective with the acoustic shroud than without it, and the resulting suppression was 14.5 EPNdB and a 14.3-percent loss in thrust coefficient. Removing the acoustic shroud reduced suppression by 2 EPNdB but did not change the thrust loss.

In the previous discussion, suppression was given in terms of a parameter called effective perceived noise level EPNL, the units of which are EPNdB. This parameter accounts for the duration of the noise as the aircraft flies past the observer, a longer duration noise being more annoying and therefore less favorable than the same noise for a shorter duration. The amount that the duration effect contributes to the suppression of the 104-tube suppressor with an acoustic shroud is shown in figure 25. Also shown are the effects that scaling and distance have on suppression. A suppression of 8.5 PNdB was achieved with the 0.23-scale suppressor when it was flown over the measuring station at an altitude of 91 meters (300 ft) and a Mach number of 0.4. Scaling up to full size resulted in a suppression of 10.3 PNdB, that is, suppression increased by 1.8 PNdB. The 0.23-scale suppressor has much more of its spectrum in the very annoying range of frequencies (2 to 5 kHZ) than does the baseline nozzle. Scaling up to full size shifted this spectrum into the lower, less annoying frequency range, which resulted in the increased

suppression. (This value of suppression might be somewhat conservative because of experimental measurement difficulties discussed later in this section.)

The effect of distance on suppression was determined by using the full-scale results extrapolated to the sideline distance of 648 meters from an altitude of 305 meters. The extrapolation resulted in a suppression of 13.5 PNdB compared to a suppression of 10.3 PNdB when the full-scale suppressor was flown at an altitude of 91 meters directly over the measuring station. So the 104-tube suppressor with the acoustic shroud benefits 3.2 PNdB by increasing the distance between the noise source and observer. The high frequencies contribute more to the perceived noise level of the suppressor configuration than they do to that of the baseline nozzle. It is the high frequencies that are rapidly attenuated by the atmosphere.

The last effect is that of time duration. Noise from the suppressor has a somewhat shorter time duration and therefore the annoyance from this factor is less, by 1 EPNdB, than in noise from the baseline nozzle.

The discussion concerning the effect of scaling on suppression mentioned that the value of suppression might be somewhat conservative. The full-scale spectrum probably is too high at frequencies above 1150 hertz because of experimental measurement difficulties associated with the 0.23 scaled (J85 size) spectrum. As mentioned in the section Acoustic Characteristics, the acoustic signal received at the microphone quite possibly is below the noise floor of the recording equipment at frequencies above 5000 hertz. Since the scaling factor is 0.23, the measured results at a frequency of 5000 hertz scale to a frequency of 1150 hertz for the full-size spectrum.

This would affect the perceived noise level of the suppressor nozzle more than that of the baseline nozzle and thereby result in an erroneously low value of suppression. The magnitude of the error can be estimated by calculating the PNL values for both the suppressor nozzle and the baseline nozzle with the assumption that the sound-pressure-level values are zero at frequencies above 1150 hertz. The calculation indicated that this error amounted to about 1 PNdB.

SUMMARY OF RESULTS

A series of flyover and static tests was conducted on a 104-tube suppressor. The effects of incorporating an acoustic shroud and of incorporating scoops also were studied. Primary jet exhaust was provided by a calibrated turbojet engine. Data were taken over a range of power settings which resulted in relative jet velocities between 381 and 537 meters per second (1250 and 1760 ft/sec) for flyover conditions. The results of the investigation at a relative jet velocity of about 537 meters per second (1760 ft/sec) can be summarized as follows:

1. Comparison of the adjusted flyover and static spectra at the acoustic angle that results in peak flyover noise indicates that flight velocity had a small adverse effect on suppression of the 104-tube suppressor. The adverse effect was slightly larger with the acoustic shroud than without it. The scoops did not change the adverse effect.

2. The variation in perceived noise level with acoustic angle during a typical flyover compared to that extrapolated from static data indicated that the peak noise level predicted from static data was lower and occurred closer to the jet axis than that obtained during the flyover of the 104-tube suppressor. When the acoustic shroud was used, the static data again predicted a lower peak noise level but predicted it to occur farther from the jet axis than those obtained during the flyover of this configuration.

3. Peak noise level of the 104-tube suppressor in flyover was about 7.5 PNdB below that of the baseline nozzle and occurred about 20° farther from the jet axis. (Peak noise level of the baseline nozzle was 118.5 PNdB and occurred at an angle of about 40°.) Incorporating the acoustic shroud resulted in a further reduction of about 2.5 PNdB in peak noise level and shifted it about 7° farther from the jet axis when compared with the base suppressor.

4. The frequency spectrum for the 104-tube suppressor in flyover contained only a small amount of low-frequency and midfrequency noise but about as much high-frequency noise as the baseline nozzle. The high-frequency noise peaked at a frequency of 3200 hertz. Incorporating the acoustical shroud resulted in lowering the spectrum level by as much as 12.5 dB at a frequency of 3200 hertz.

5. The thrust coefficient for flyover at a nozzle pressure ratio of 2.4 was not adversely affected by incorporating the acoustic shroud. For static conditions at a nozzle pressure ratio of 2.1, the thrust coefficient increased about 2 percent when the acoustic shroud was installed.

6. The acoustic data from the flyover tests were scaled up from J85 engine size (0.23 scale) to full scale and then extrapolated to a sideline distance of 648 meters (2128 ft) from an altitude of 305 meters (1000 ft). The results showed that the 104-tube suppressor with the acoustic shroud reduced the peak noise level by 14.5 EPNdB (relative to the baseline nozzle). This was achieved with a thrust penalty of 14.3 percent, which made it the most effective of the 104-tube suppressor configurations tested.

Lewis Research Center,
National Aeronautics and Space Administration,
Cleveland, Ohio, March 27, 1974,
501-24.

APPENDIX A

AIRCRAFT LOCATION

As the aircraft flies over the microphone, a time history of the noise is recorded on tape. Each instant of time is associated with a particular location of the aircraft. This relation was established by determining the time associated with the point of closest approach. The method for accomplishing this is described in this appendix, which also describes how the flyover altitude was determined and how the measured sound pressure level was adjusted to that recorded had the aircraft flown directly over the microphone at an altitude of 91 meters (300 ft).

The technique required a camera located close to the microphone and an observer stationed about 68 meters (220 ft) upstream of the camera, as shown schematically in figure 26(a). The observer recorded a 14-kilohertz tone on the tape when the aircraft flew over him. After a 0.5-second time delay, during which the aircraft traveled the 68 meters from the observer to the camera, the camera recorded a picture and a second 14-kilohertz tone was automatically recorded on the tape. The time interval between the first and second tones served as a check on the accuracy of the time delay. A typical picture taken by the camera is shown schematically in figure 26(b). The average size parameters X_{is}, $(WL)_{is}$, and Y_{is} were measured from the photograph to an accuracy of ±0.006 centimeter (0.0025 in.), accounting for distortion of the camera lens.

The image size parameters X_{is} and $(WL)_{is}$ were used to determine the time associated with the closest approach. To illustrate this use, a typical time history of the perceived noise level is shown in figure 26(c). The time for the aircraft to travel from the location where the picture was taken to the location of closest approach is given by

$$T_{pe} = \frac{l_{pc}}{V_a} \tag{A1}$$

The actual ground distance l_{pc} was determined from the image ground distance X_{xs}, the image length of the wing $(WL)_{is}$, and the actual length of the wing WL by the equation

$$l_{pc} = X_{is} \frac{WL}{(WL)_{is}} \tag{A2}$$

When l_{pc} from equation (A2) is substituted into equation (A1), the expression for T_{pe} becomes

$$T_{pe} = \frac{WL(X_{is})}{V_a(WL)_{is}} \tag{A3}$$

Thus, the time associated with the closest approach of the aircraft T_{ca} after the 14-kilohertz tone is

$$T_{ca} = T_{TD} + T_{pe} \tag{A4}$$

It is required that an integration period begin precisely at the time of closest approach. Each integration period is the sum of the time to integrate t_i and the time to read the data out of the analyzer t_{ro}. If N of these periods occur before closest approach, the time from the beginning of the first integration period to the one before closest approach becomes

$$T_{ica} = N(t_i + t_{ro}) \tag{A5}$$

This time interval cannot be greater than the time interval T_{ca} (eq. (A4)), since it is not practical to start the first integration period before the time of the 14-kilohertz tone. Since the time interval T_{ica} generally will not be exactly the same as the time interval T_{ca} it will be necessary to delay the start of the first integration period by a time T_D, so that

$$T_D + T_{ica} = T_{ca} \tag{A6}$$

When T_{ica} from equation (A5), T_{ca} from equation (A4), and T_{pe} from equation (A3) are substituted into equation (A6), the expression for T_D becomes

$$T_D = T_{TD} + \frac{WL(X_{is})}{V_a(WL)_{is}} - N(t_i + t_{ro}) \tag{A7}$$

All the parameters on the right side of the equation are shown except N. The value of N is chosen such that the resulting value of T_D is less than one integration period and the resulting sign of T_D is positive.

In addition to determining the time associated with the closest approach, the altitude of the aircraft also was determined by using the camera. This is shown in figure 26(d). Altitude H was determined from the image length of the wing $(WL)_{is}$, the actual length of the wing WL, the focal length of the camera FL, and the height of the camera above the concrete surface h_m:

$$H = h + FL \frac{WL}{(WL)_{is}} \tag{A8}$$

This method allows the altitude to be determined to within ±1.5 meters (±5 ft).

Small differences in the aircraft altitude H and its lateral location Y occurred from flyover to flyover. The geometry is shown in figure 26(e). The altitude H was determined from equation (A8). Lateral location Y was determined from the image lateral location Y_{is} (see fig. 26(b)), the image length of the wing $(WL)_{is}$, and the actual length of the wing WL.

$$Y = Y_{is} \frac{WL}{(WL)_{is}} \tag{A9}$$

As a result of the small differences in altitude and lateral location, the direct ray distance from the noise source to the microphone R_p' varied from flyover to flyover (for the same acoustic angle θ). This deviation, in turn, caused differences in the level of the noise received at the microphone for a constant noise level emitted at the source. To eliminate these variations, the noise levels were adjusted to what would be recorded had the aircraft flown directly over the microphone at an altitude of 91 meters (300 ft). This was done by adjusting the recorded noise level at each acoustic angle by an amount $(\Delta\ dB)_\theta$, given by

$$(\Delta\ dB)_\theta = 20 \log \left(\frac{R_p'}{R_p} \right)_\theta \tag{A10}$$

APPENDIX B

BASEPLATE PRESSURES

Static Conditions

The pressure distribution on the baseplate at static conditions is shown in figure 27. Without the acoustic shroud, there is no significant circumferential variation in static pressure on the baseplate either above or below the outer row of tubes (fig. 27(a)). So there is probably no circumferential variation of static pressure in any of the other rows of tubes either. However, there is a large variation of static pressure in the radial direction (fig. 27(b)). Static pressure decreases rapidly towards the inner rows of tubes and reaches a minimum below the row of tubes that has the largest exit area. Thus, the baseplate is not adequately ventilated even though the major axis of the elliptical tubes was oriented radially in an effort to achieve good ventilation. Installing the acoustic shroud resulted in lowering the static pressures on the baseplate at all radial locations and thereby increasing the pressure drag; the ratio of pressure drag to ideal primary thrust increased to 0.104 from 0.056 (fig. 27(c)). These results were for a constant pressure ratio of 2.26. Decreasing the pressure ratio resulted generally in an increase in the static pressures at all radial locations and, consequently, a decrease in the drag on the baseplate (fig. 27(d)). The radial variation is shown only for the suppressor without the shroud, but it is typical of that obtained with the acoustic shroud. For both configurations the ratio of pressure drag to ideal primary thrust remained fairly constant as pressure ratio decreased from 2.2 to 1.8 but then increased at lower pressure ratios (fig. 27(d)).

Flyover Conditions

The pressure distribution on the baseplate is shown in figure 28. Without the acoustic shroud, there is a circumferential variation in static pressure on the baseplate (fig. 28(a)). The static pressure, as expected (refs. 11, 20, and 21), was high near the top of the baseplate (0°) and low near the bottom (180°) because of the presence of the wing. This variation was evident at both radial locations (i.e., at 26.85 and 21.59 cm). (At static conditions, no circumferential variation in pressure was evident.)

In addition to the circumferential variation, there is also a radial variation in static pressure on the baseplate (fig. 28(b)). The lowest static pressure occurred inside the row of tubes that had the largest exit area. (This is the same radial location where the lowest pressure occurred at static conditions.) Thus, the baseplate was not adequately ventilated in flyover.

The results presented so far were for a constant corrected secondary weight flow ratio of 0.06 (at static conditions, there was essentially no secondary flow) and a suppressor with no shroud. Decreasing the corrected secondary weight flow ratio to about 0.03 did not significantly affect the radial variation of static pressure on the baseplate (fig. 28(c)). Installing the acoustic shroud, however, resulted in increasing the static pressures on the baseplate (fig. 28(d)) and thereby improving ventilation. The static-pressure increase, which was small at all radial locations except 21.59 centimeters, resulted in decreasing the ratio of pressure drag to ideal primary thrust to 0.078 from 0.092.

Scoops were installed on the suppressor configuration with the acoustic shroud. This addition resulted in a further small increase in the static pressure at most radial locations (fig. 28(d)). The increase, which was most noticeable at the 11.23-centimeter radial location, resulted in only a slight decrease in the ratio of pressure drag to ideal primary thrust to 0.073 from 0.078. Thus, installing the scoops did not result in a marked improvement in ventilation.

These results were for a constant pressure ratio of 2.53. Decreasing the pressure ratio generally resulted in increasing the static pressure at all radial locations and, consequently, decreasing the drag on the baseplate (fig. 28(e)). Ventilation also improved with decreasing pressure ratio. The radial variation is shown only for the suppressor configuration without the acoustic shroud, but it is typical of those obtained with the other configurations. Even though pressure drag on the baseplate decreased with decreasing pressure ratio for all configurations, the ideal primary thrust decreased more rapidly. This difference resulted in an increasing ratio of pressure drag to ideal primary thrust with decreasing pressure ratio (fig. 28(e)).

Effect of Flight Velocity

The effect of flight velocity on the ratio of baseplate pressure drag to ideal primary thrust is shown in figure 29 as a function of exhaust nozzle pressure ratio. Figure 29(a) shows the effect for the suppressor configuration without the acoustic shroud. Flight velocity had a large adverse effect over the entire range of pressure ratios. At a pressure ratio of 2.3, the ratio of pressure drag to ideal thrust increased from 0.054 for static conditions to 0.103 for flyover conditions; at a pressure ratio of 1.7, the increase was from 0.064 to 0.138. This variation indicates that ventilation was much worse for flyover than for static conditions.

Figure 29(b) shows the flight velocity effect for the suppressor configuration with the acoustic shroud. Flight velocity had a beneficial effect at the higher pressure ratios but a negligible effect at the lower pressure ratios. At a pressure ratio of 2.3, the ratio of pressure drag to ideal primary thrust decreased from 0.105 for static conditions to 0.86

for flyover conditions; at a pressure ratio of 1.9, the decrease was from 0.11 to 0.104. These values indicate that ventilation was better for flyover than for static conditions especially at the higher pressure ratios.

REFERENCES

1. Darchuk, George V.; and Balombin, Joseph R.: Noise Evaluation of Four Exhaust Nozzles for Afterburning Turbojet Engines. NASA TM X-2014, 1970.

2. Huff, Ronald G.; and Groesbeck, Donald E.: Splitting Supersonic Nozzle Flow Into Separate Jets By Overexpansion Into a Multilobed Divergent Nozzle. NASA TN D-6667, 1972.

3. Ciepluch, Carl C.; North, Warren J.; Coles, Willard D.; and Antl, Robert J.: Acoustic, Thrust, and Drag Characteristics of Several Full-Scale Noise Suppressors for Turbojet Engines. NACA TN 4261, 1958.

4. Brausch, J. F.: Flight Velocity Influence on Jet Noise of Conical Ejector, Annular Plug, and Segmented Suppressor Nozzles. General Electric Co. (NASA CR-120961), 1972.

5. Burley, Richard R.; and Karabinus, Raymond J.: Flyover and Static Tests to Investigate External Flow Effect on Jet Noise for Nonsuppressor and Suppressor Exhaust Nozzles. NASA TM X-68161, 1972.

6. Burley, Richard R.; Karabinus, Raymond J.; and Freedman, Robert J.: Flight Investigation of Acoustic and Thrust Characteristics of Several Exhaust Nozzles Installed on Underwing Nacelles on an F-106 Aircraft. NASA TM X-2854, 1973.

7. Burley, Richard R.; and Johns, Albert L.: Flight Velocity Effects on Jet Noise of Several Variations of a Twelve-Chute Suppressor Installed on a Plug Nozzle. NASA TM X-2918, 1974.

8. Burley, Richard R.; and Head, Verlon L.: Flight Velocity Effects on the Jet Noise of Several Variations of a 48-Tube Suppressor Installed on a Plug Nozzle. NASA TM X-2919, 1974.

9. Chamberlin, Roger: Flyover and Static Tests to Study Flight Velocity Effects on Jet Noise of Suppressed and Unsuppressed Plug Nozzle Configurations. NASA TM X-2856, 1973.

10. Swan, Walter C.; and Simcox, Craig, D.: A Status Report on Jet Noise Suppression as Seen by an Aircraft Manufacturer. Presented at the International Symposium on Air Breathing Engines, 1st, Marseille, France, June 19-23, 1972.

11. Samanich, Nick E.; and Chamberlin, Roger: Flight Investigation of Installation Effects on a Plug Nozzle Installed on an Underwing Nacelle. NASA TM X-2295, 1971.

12. Mangiarotty, R. A.; Marsh, Alan H.; and Feder, Ernest: Duct-Lining Materials and Concepts. Progress of NASA Research Relating to Noise Alleviation of Large Subsonic Jet Aircraft. NASA SP-189, 1968, pp. 29-52.

13. Groth, Harold W.; Samanich, Nick E.; and Blumenthal, Philip Z.: Inflight Thrust Measuring System for Underwing Nacelles Installed on a Modified F-106 Aircraft. NASA TM X-2356, 1971.

14. Antl, Robert J.; and Burley, Richard R.: Steady-State Airflow and Afterburning Performance Characteristics of Four J85-GE-13 Turbojet Engines. NASA TM X-1742, 1969.

15. Little, John W.; Miller, Robert L.; Oncley, Paul B.; and Panko, Raymond E.: Studies of Atmospheric Attenuation of Noise. NASA Acoustically Treated Nacelle Program, NASA SP-220, 1969, pp. 125-135.

16. Blumenthal, V. L.; Streckenbach, J. M.; and Tate, R. B.: Aircraft Environmental Problems. Paper 73-5, AIAA, Jan. 1973.

17. Grande, Edvard: Exhaust Noise Field Generated in the JT8D Core Engine-Noise Floor Presented by the Internal Noise Source. Presented at the Acoustical Society of America 82nd Fall Meeting, Denver, Colo., Oct. 19-22, 1971.

18. Jet Noise Prediction. Aerospace Information Rep. 876, SAE, July 10, 1965.

19. Federal Aviation Regulations, Volume III, Part 36, Noise Standards: Aircraft Type Certification. Dept. of Transportation, Federal Aviation Administration.

20. Burley, Richard R.: Flight Investigation of Airframe Installation Effects on an Auxiliary Inlet Ejector Nozzle on an Underwing Engine Nacelle. NASA TM X-2396, 1971.

21. Mikkelson, Daniel C.; and Head, Verlon L.: Flight Investigation of Airframe Installation Effects on a Variable Flap Ejector Nozzle of an Underwing Engine Nacelle at Mach Numbers from 0.5 to 1.3. NASA TM X-2010, 1970.

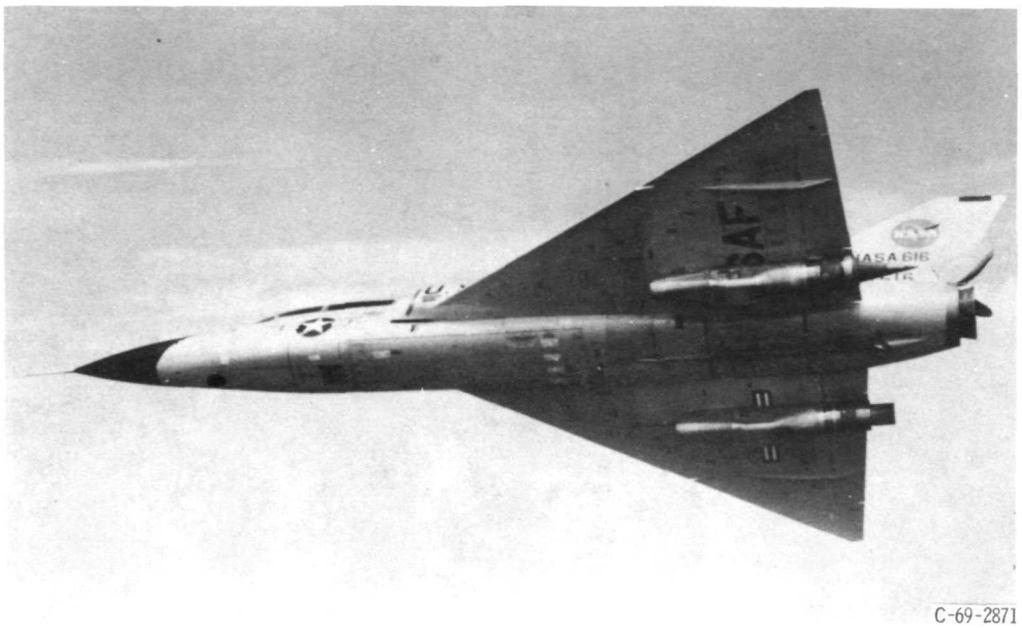

Figure 1. - Modified F-106B aircraft in flight.

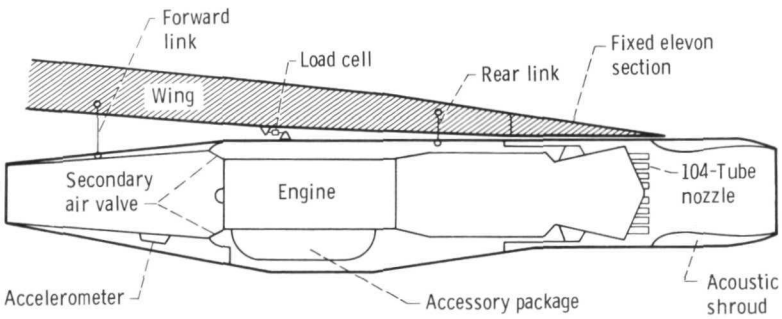

Figure 2. - Nacelle-engine installation.

Figure 3. - Nacelle modification for static tests.

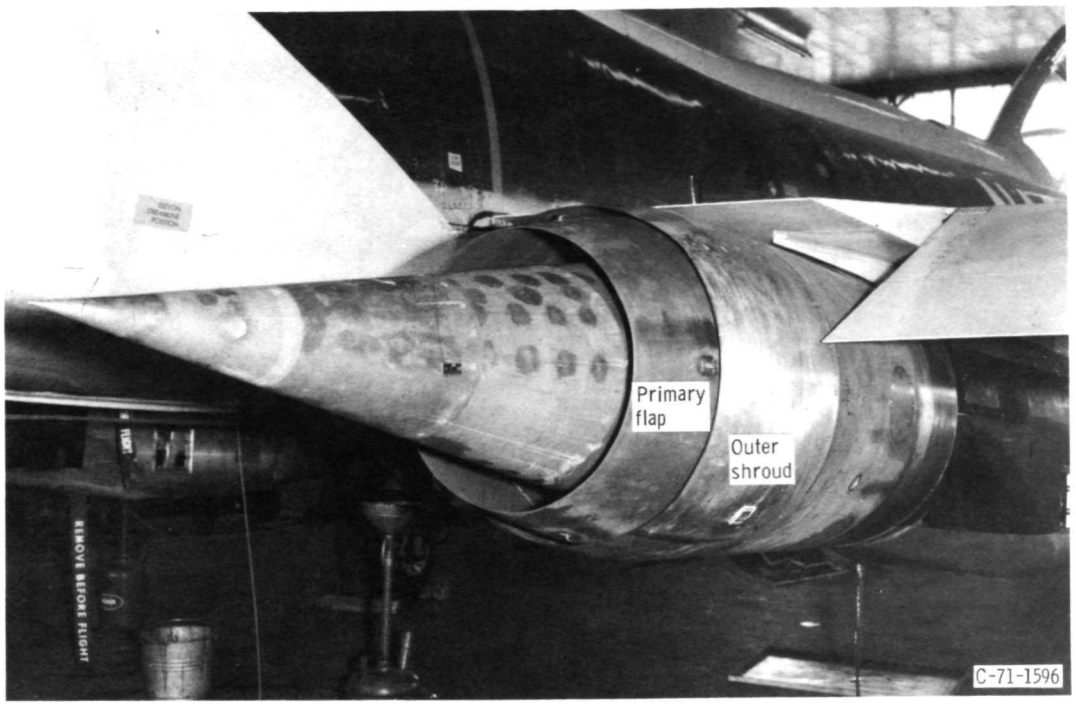

(a) Installed.

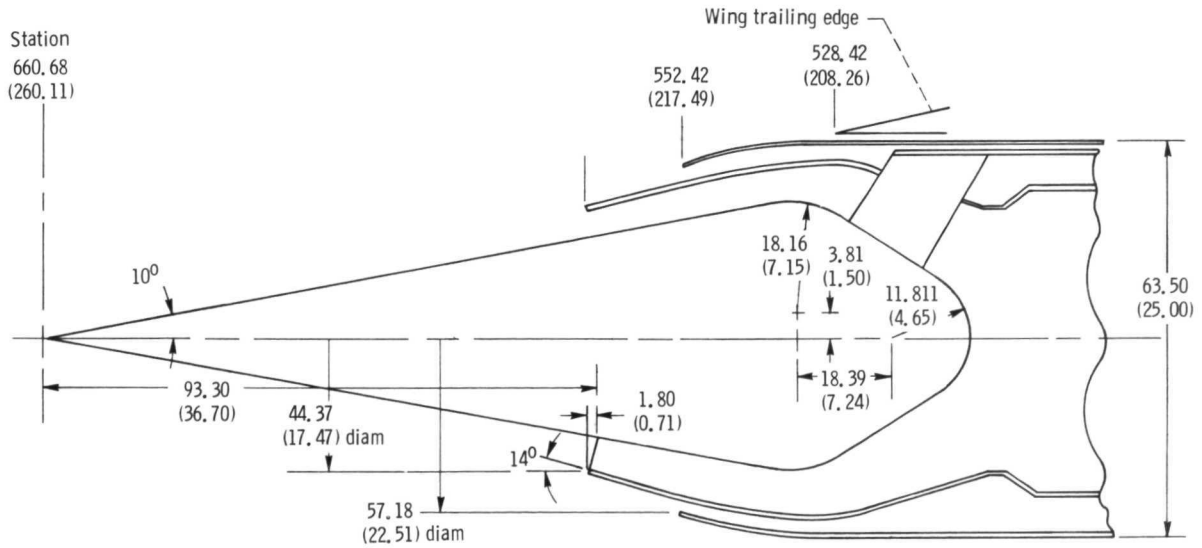

(b) Dimensional characteristics. (Dimensions are in centimeters (in.); station numbers are based on a compressor inlet station number of 254 (100).)

Figure 4. - Baseline nozzle.

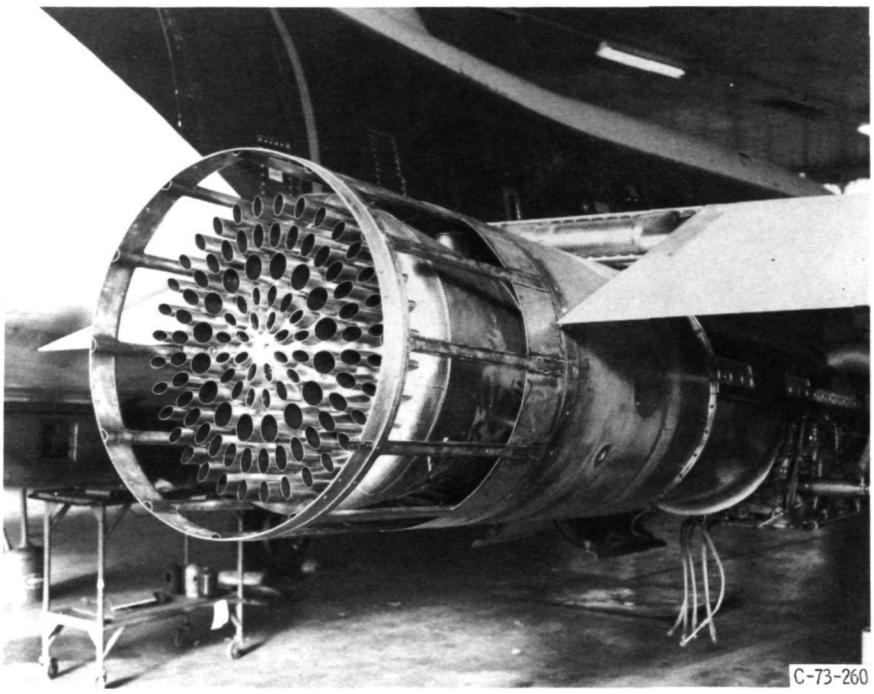

(a) 104-Tube nozzle; overall view.

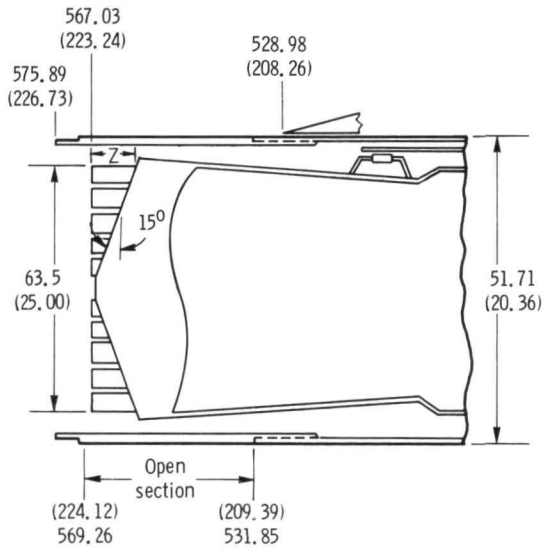

(b) 104-Tube nozzle; dimensional characteristics.

Figure 5. - Suppressor configurations. (Dimensions are in centimeters (in.).)

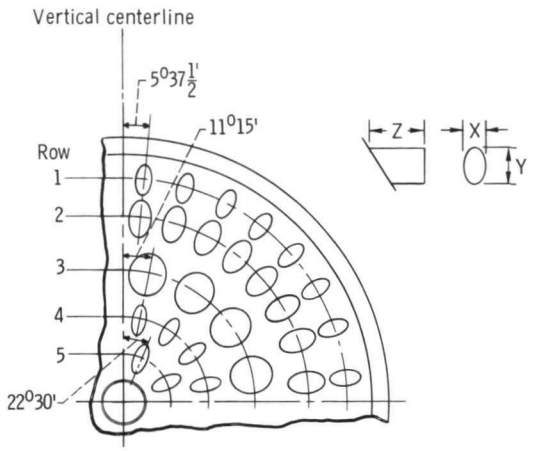

Row	Diameter of row		Tubes equally spaced	X		Y		Z	
	in.	cm		in.	cm	in.	cm	in.	cm
1	18.96	48.16	32	0.77	1.96	1.40	3.56	3.63	9.22
2	15.00	38.10	32	.96	2.44	1.63	4.14	3.00	7.62
3	10.84	27.53	16	1.44	3.66	1.82	4.62	2.34	5.94
4	6.84	17.37	16	.77	1.96	1.40	3.56	1.60	4.06
5	3.64	9.25	8	.77	1.96	1.40	3.56	1.06	2.69

(c) 104-Tube nozzle; tube details.

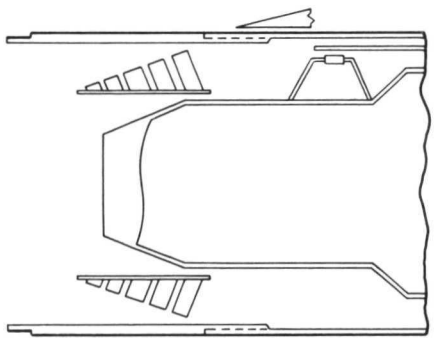

(d) 104-Tube nozzle; suppressor location for unsuppressed operation.

Figure 5. - Continued.

(e) 104-Tube nozzle with acoustic shroud; overall view.

Perforated plate				
Open area ratio	Hole diameter		Thickness	
	in.	cm	in.	cm
0.23	0.078	0.198	0.0312	0.079

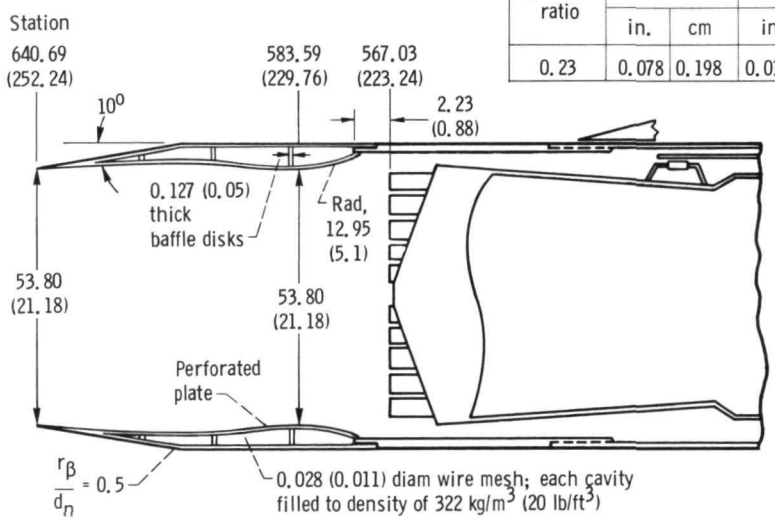

(f) 104-Tube nozzle with acoustic shroud; dimensional characteristics.

Figure 5. - Continued.

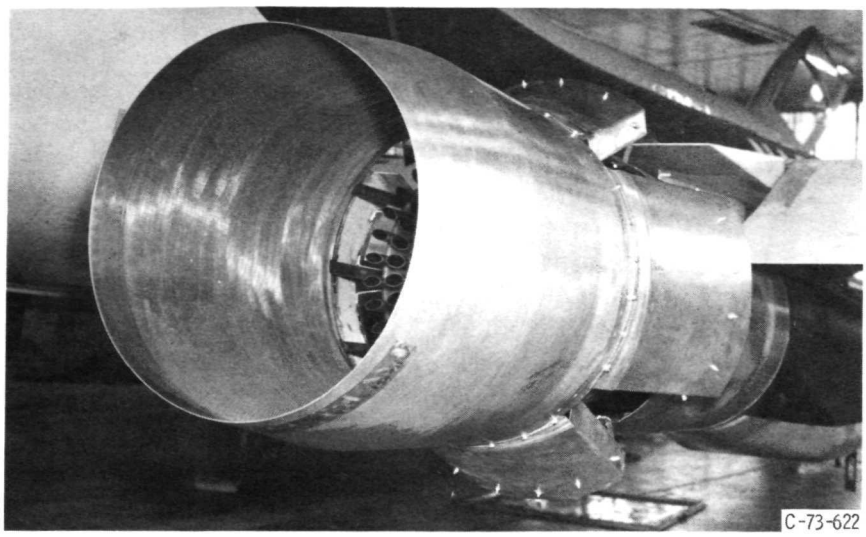

(g) 104-Tube nozzle with scoops and acoustic shroud; overall view.

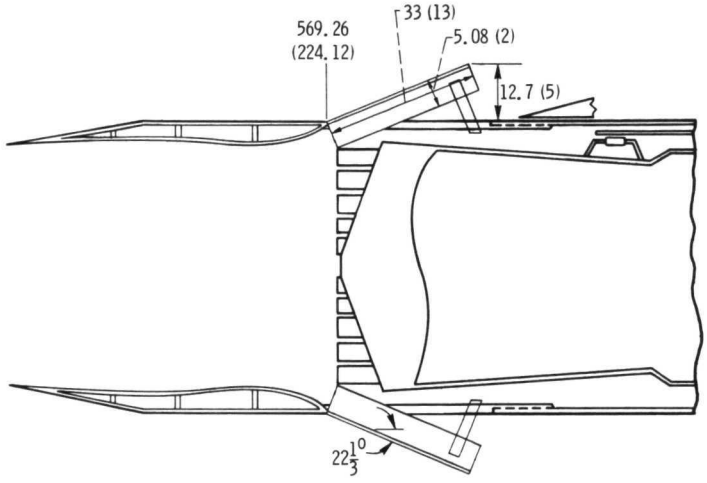

(h) 104-Tube nozzle with scoops and acoustic shroud; dimensional characteristics.

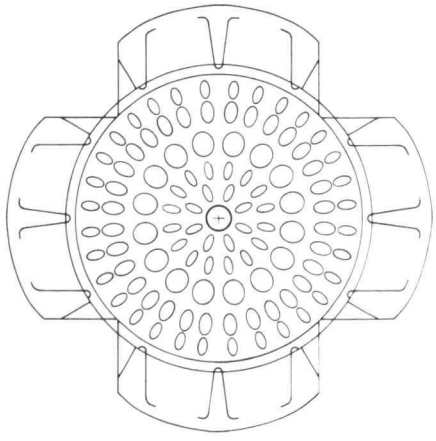

(i) 104-Tube nozzle with scoops and acoustic shroud; scoop orientation relative to tubes.

Figure 5. - Concluded.

(a) Camera.

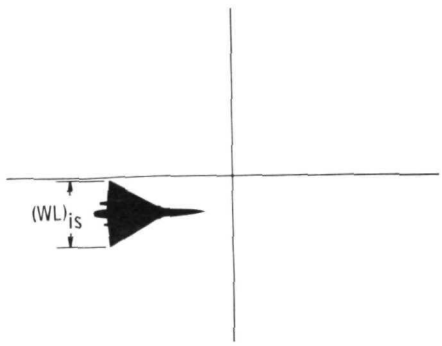

(b) Typical photograph.

Figure 6. - Technique for determining aircraft altitude.

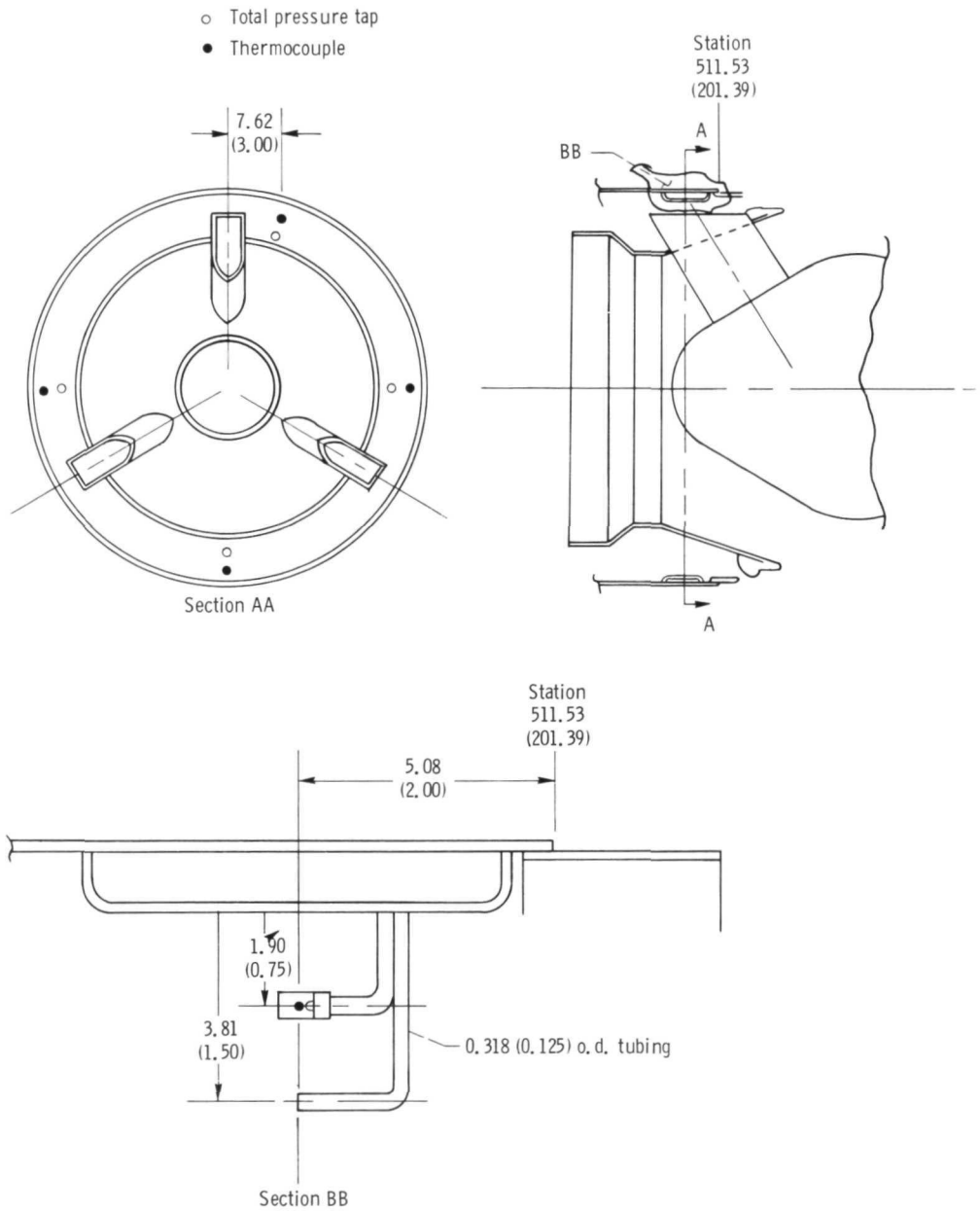

Figure 7. - Secondary passage instrumentation (dimensions in centimeters (in.)).

Tap	Location		
	Radial		Circumferential, deg
	in.	cm	
1	10.57	26.85	0
2	8.5	21.59	11.25
3	6.46	16.41	22.50
4	4.42	11.23	45
5	2.64	6.71	90
6	1.41	3.58	135
7	10.57	26.85	45
8	8.5	21.59	168.75
9	10.57	26.85	180
10	10.57	26.85	225

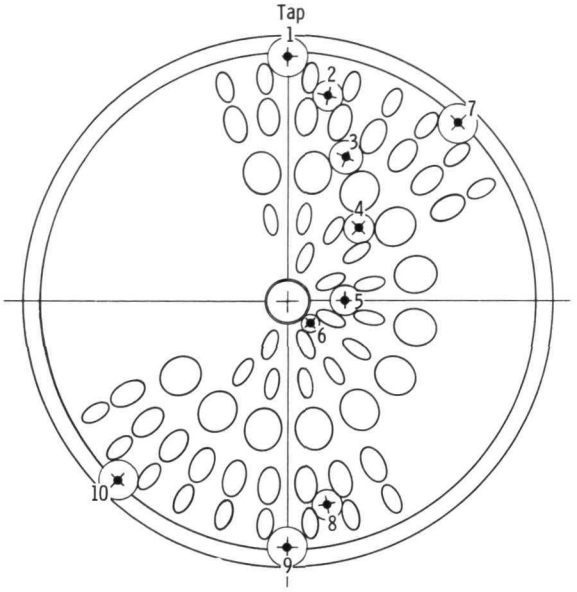

Taps are equally spaced between tubes and equally spaced between tubes and surface edges as indicated by circles

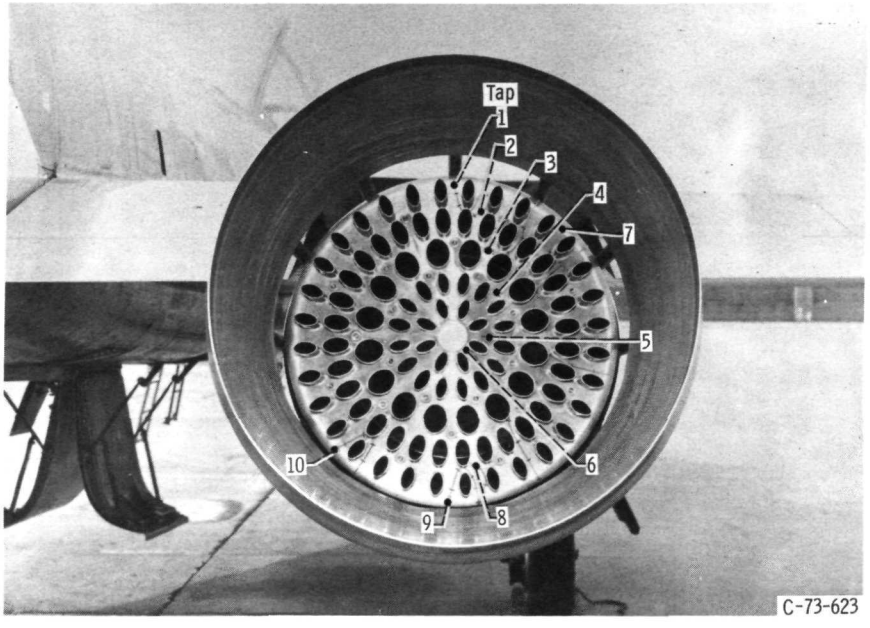

Figure 8. - Location of static-pressure taps on baseplate.

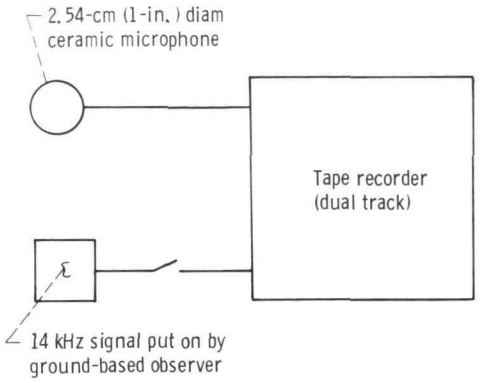

(a) Recording system for both static and flyover tests.

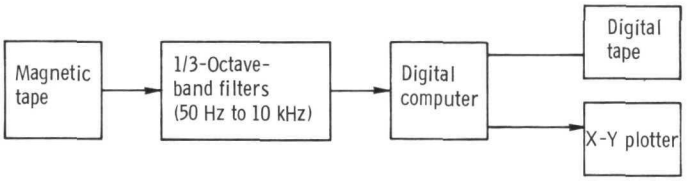

(b) Playback system for flyover tests.

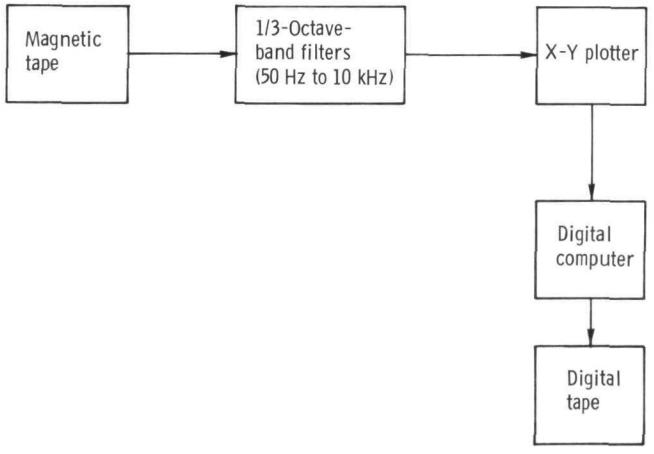

(c) Playback system for static tests.

Figure 9. - Schematic flow diagrams for noise recording system and data reduction for both static and flyover tests.

(a) Microphone orientation.

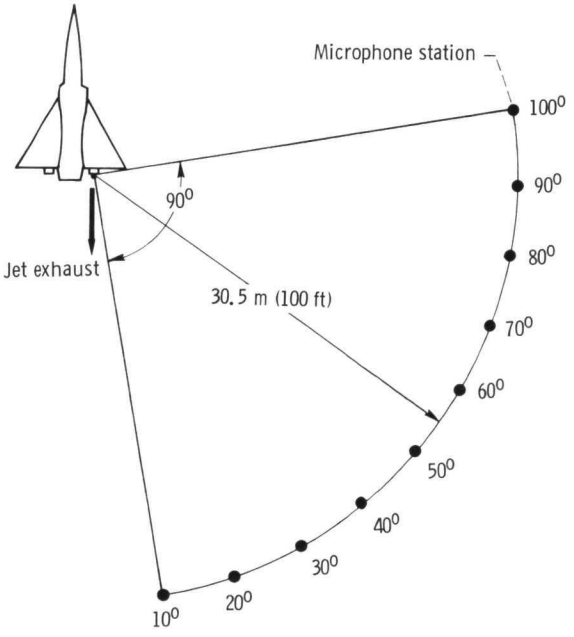

(b) Microphone location.

Figure 10. - Microphone orientation and location for static tests.

Figure 11. - Location of external source of cooling air for static tests.

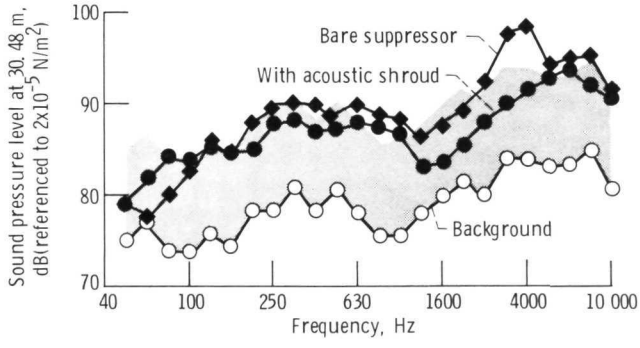

Figure 12. - Comparison of static spectra for background noise and suppressor noise. Spectra adjusted to standard day and free-field conditions; one-third-octave bands; 70° acoustic angle.

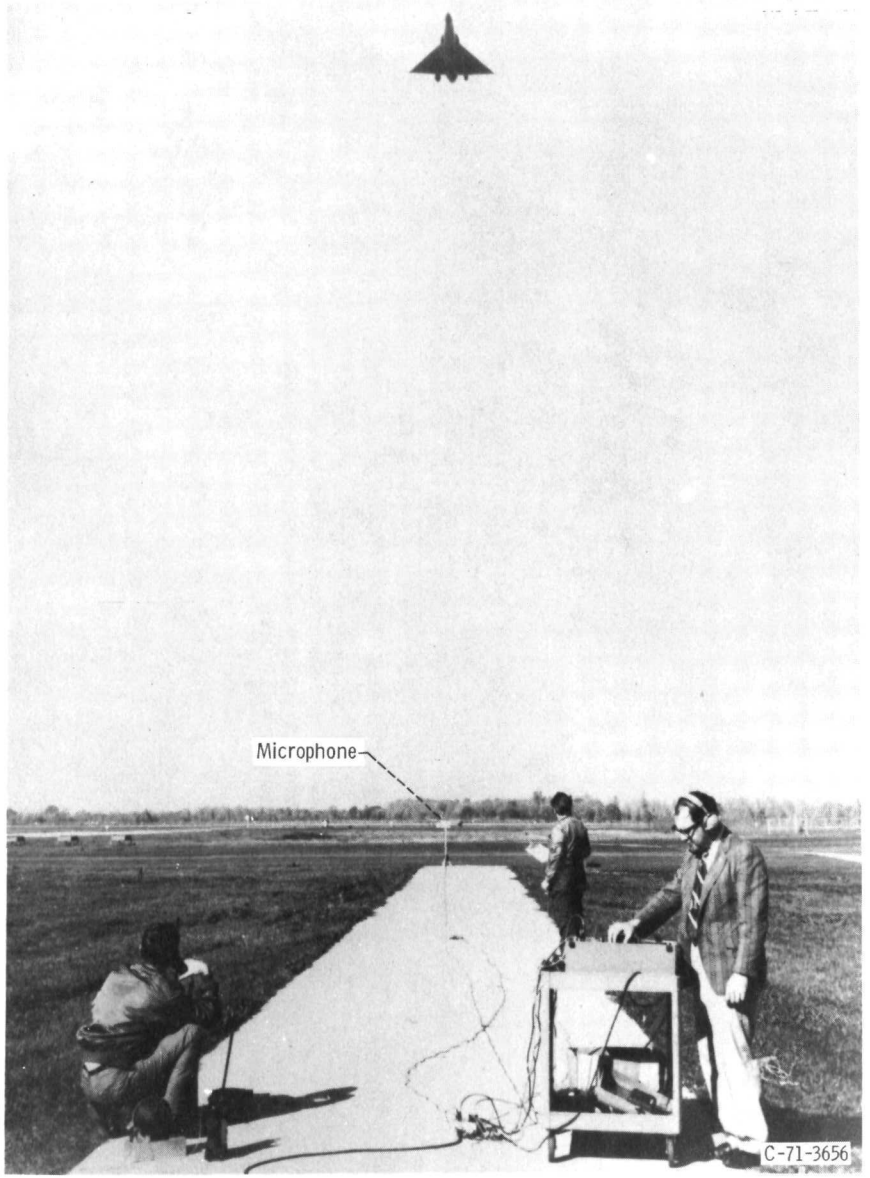

(a) Microphone orientation.

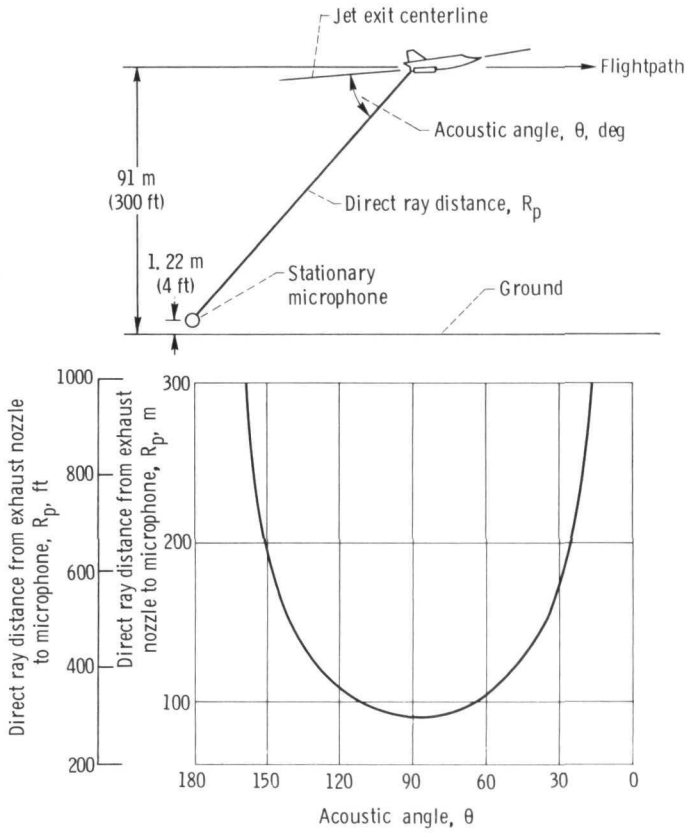

(b) Geometry.

Figure 13. - Microphone orientation and geometry for flyover tests.

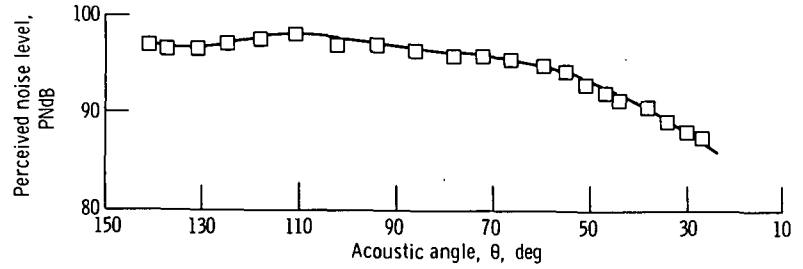

(a) Perceived noise level for 91-meter altitude.

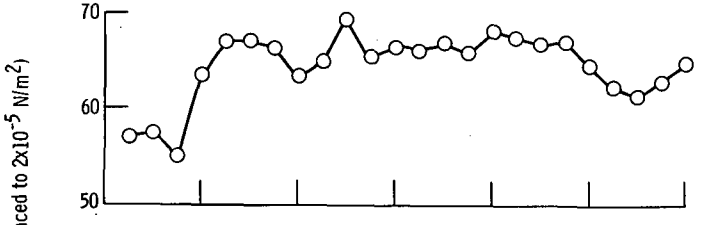

(b) 1/3-Octave-band spectra at 91-meter altitude and 40^0 acoustic angle.

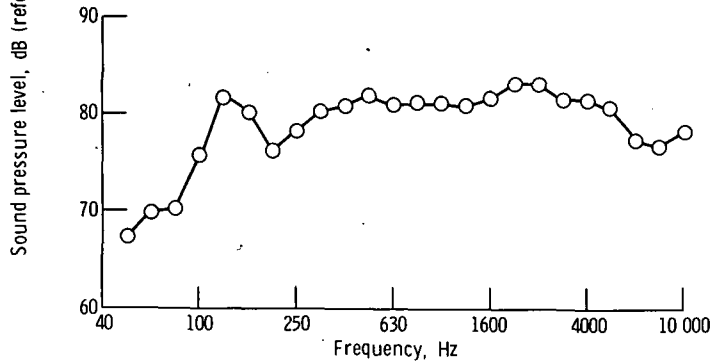

(c) 1/3-Octave-band spectra at 30.48-meter radius and 70^0 acoustic angle.

Figure 14. - Background noise for flyover.

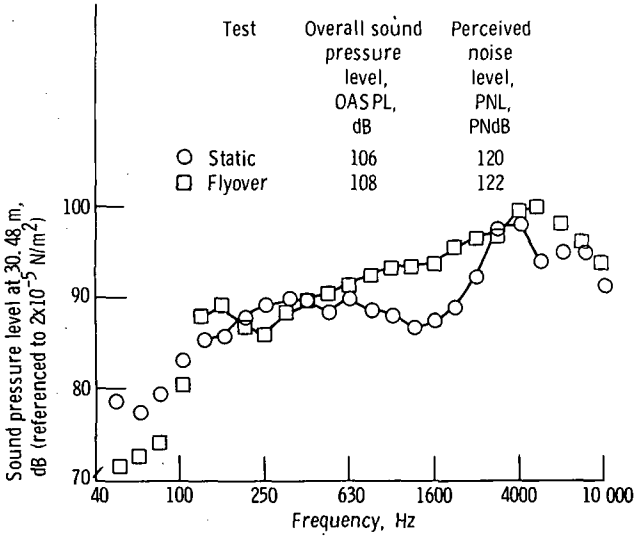

Figure 15. - Comparison of flyover and static spectra for 104-tube suppressor. Relative jet velocity, 536 meters per second (1760 ft/sec); angle of peak flyover noise, 70^0; 1/3-octave bands.

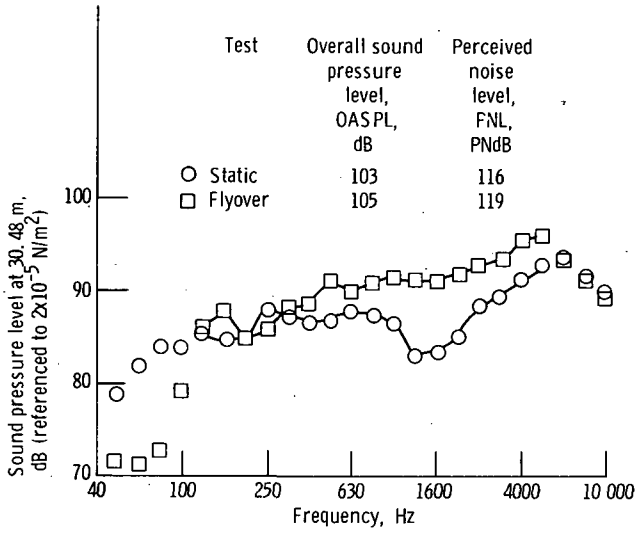

Figure 16. - Comparison of flyover and static spectra for 104-tube suppressor with acoustic shroud. Relative jet velocity, 536 meters per second (1760 ft/sec); angle of peak flyover noise, 70°; 1/3-octave bands.

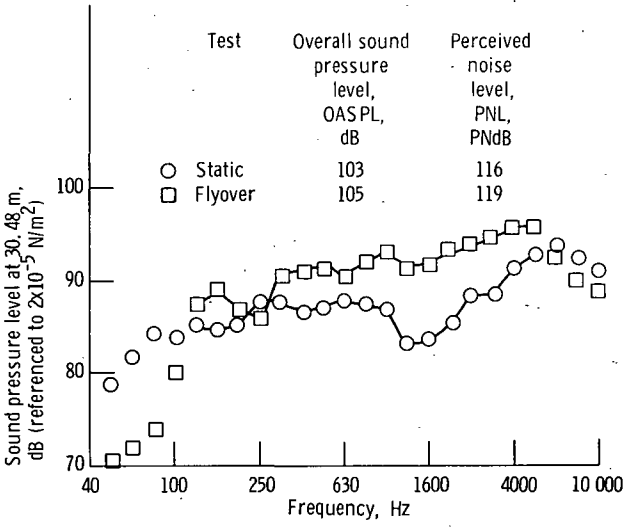

Figure 17. - Comparison of flyover and static spectra for 104-tube suppressor with scoops and acoustic shroud. Relative jet velocity, 536 meters per second (1760 ft/sec); angle of peak flyover noise, 70°; 1/3-octave bands.

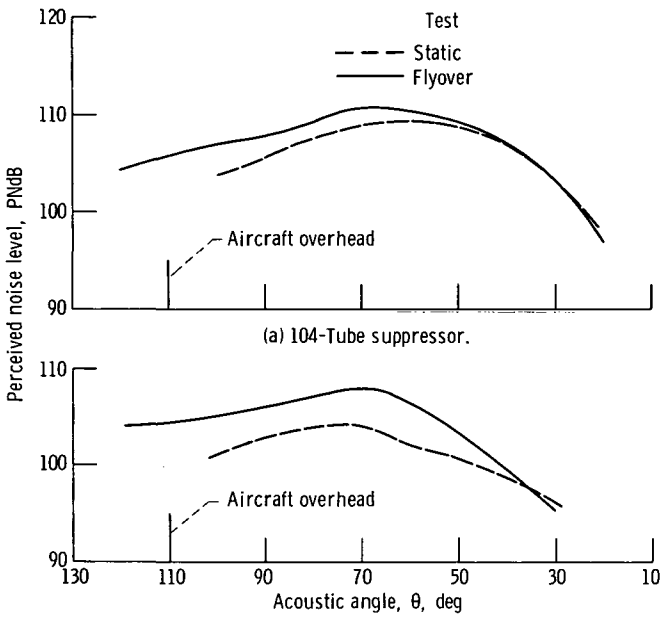

(b) 104-Tube suppressor with acoustic shroud.

Figure 18. - Flyover and static noise directivity. Relative jet velocity, 536 meters per second (1760 ft/sec); sideline/altitude, 91 meters; free field; standard day.

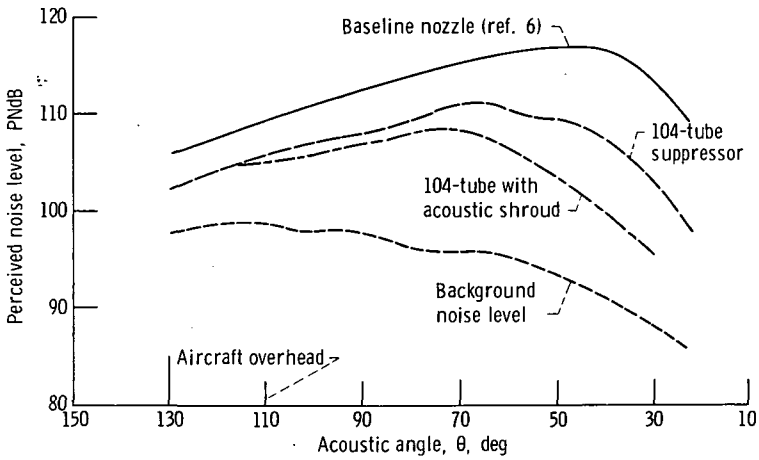

Figure 19. - Flyover noise levels directly beneath flight path. Relative jet velocity, 537 meters per second (1760 ft/sec); altitude, 91 meters; free field; standard day.

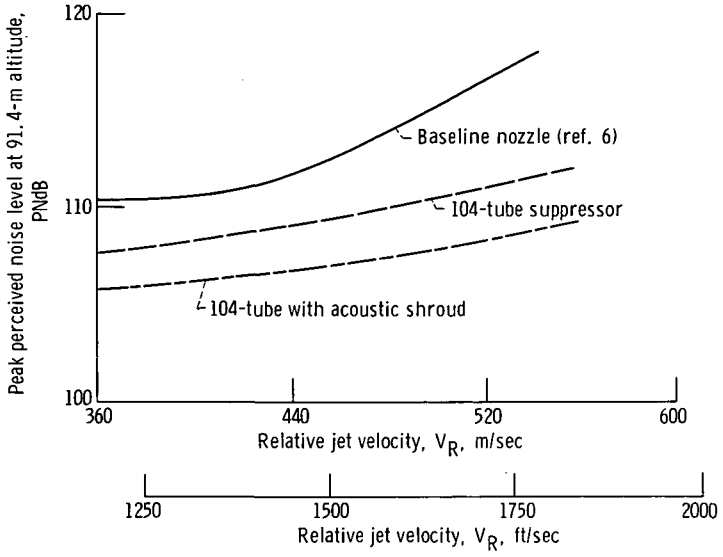

Figure 20. - Effect of relative jet velocity on peak flyover noise level.

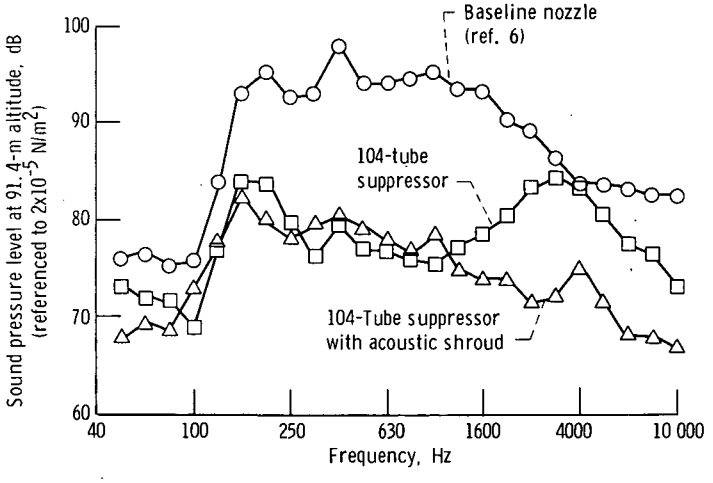

Figure 21. - Flyover spectra. Relative jet velocity, 502 meters per second; angle of peak noise for baseline nozzle, 40°; 1/3-octave bands.

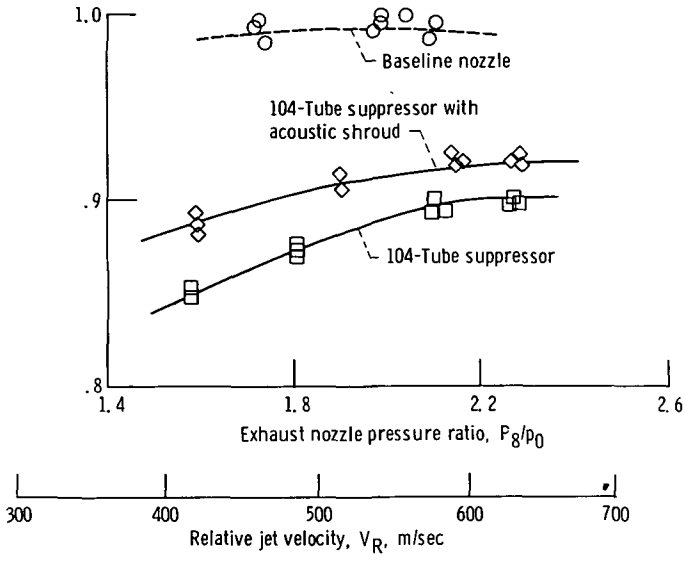

(a) Static tests.

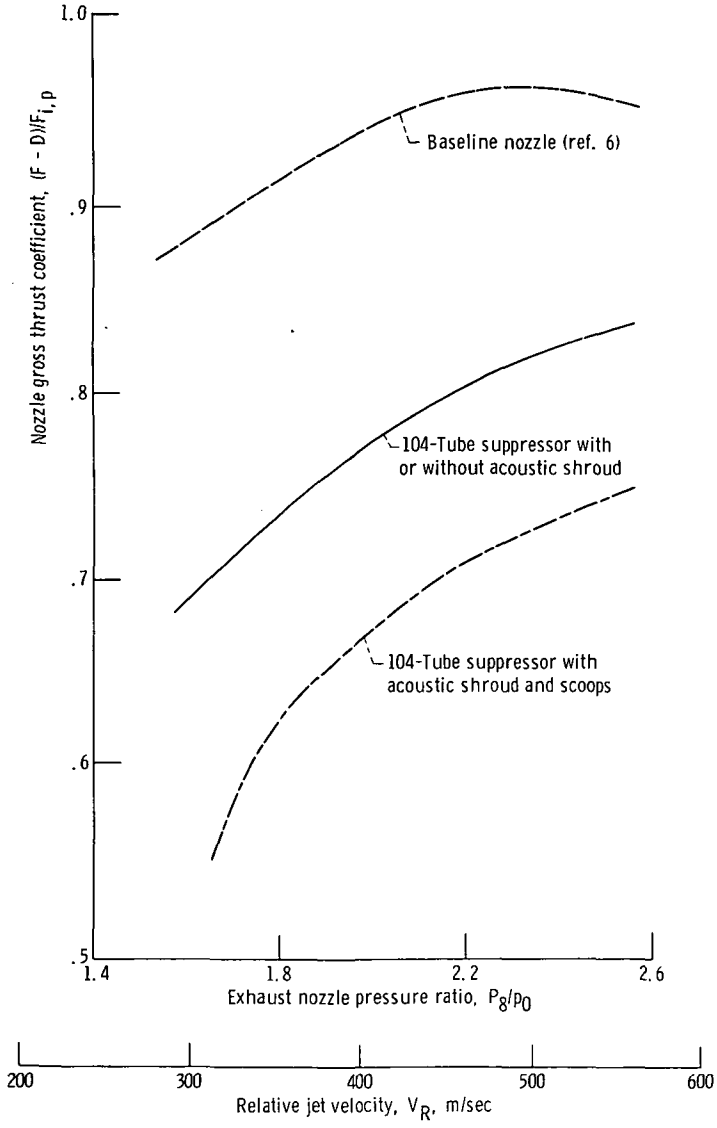

(b) Flyover tests; flight Mach number, 0.4; corrected secondary weight flow ratio, 0.06.

Figure 22. - Thrust coefficients.

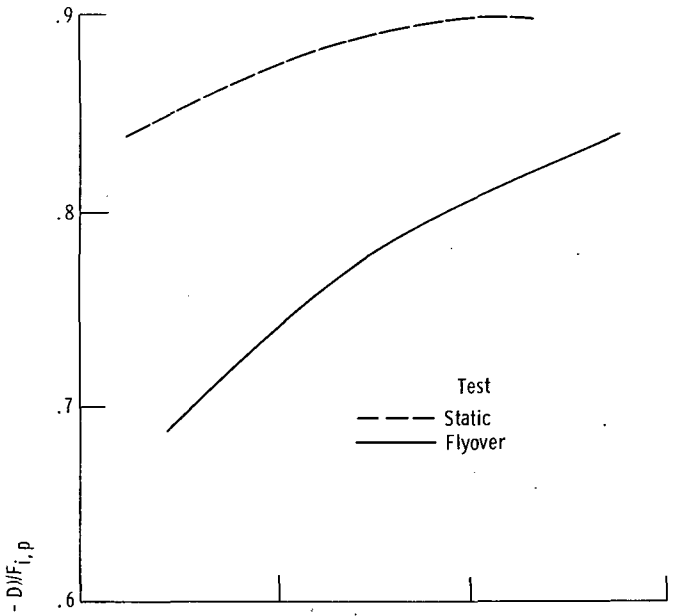

(a) 104-Tube suppressor.

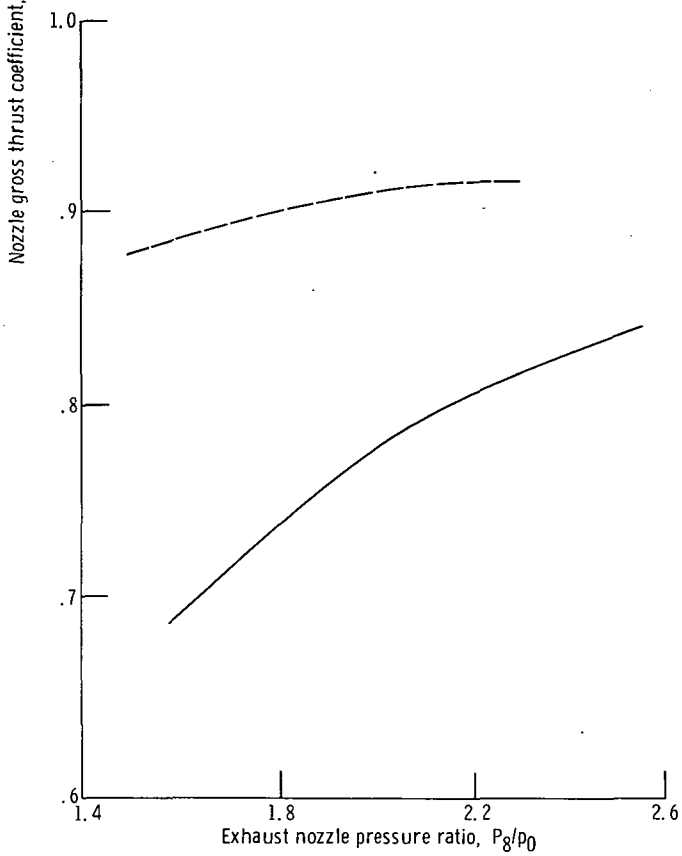

(b) 104-Tube suppressor with acoustic shroud.

Figure 23. - Effect of flight velocity on thrust of suppressor configurations.

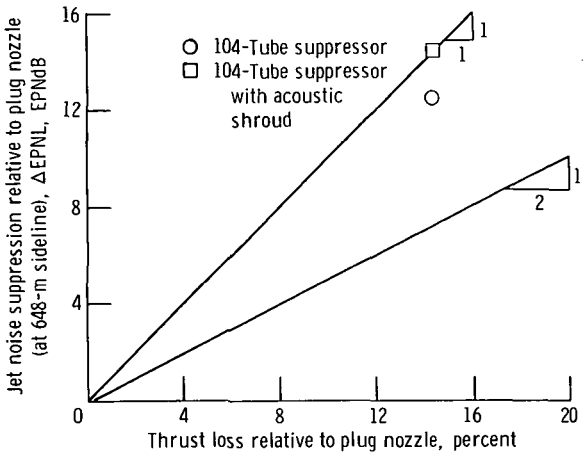

Figure 24. - Suppressor effectiveness. Flyover results scaled up to four 267-kilonewton-thrust engines; relative jet velocity, 537 meters per second (1760 ft/sec); corrected secondary weight flow ratio, 0.06; flight Mach number.

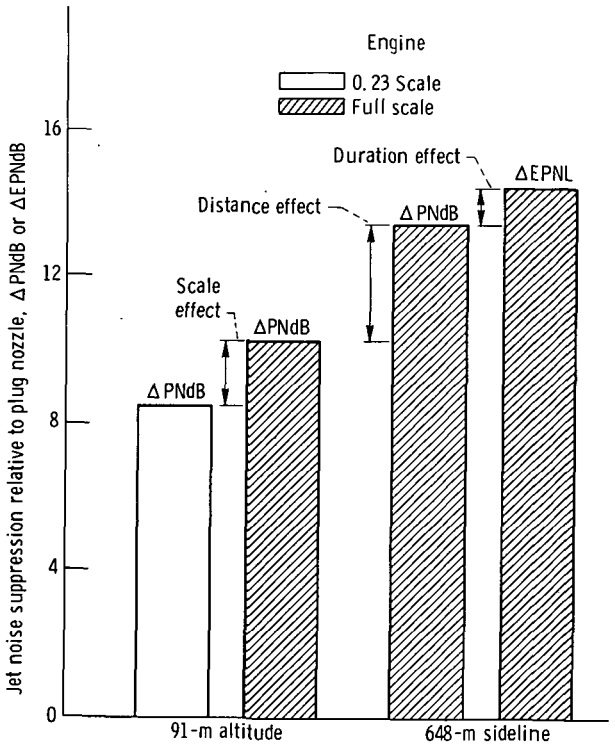

Figure 25. - Effect of scale, distance, and duration on suppression of 104-tube suppressor with acoustic shroud.

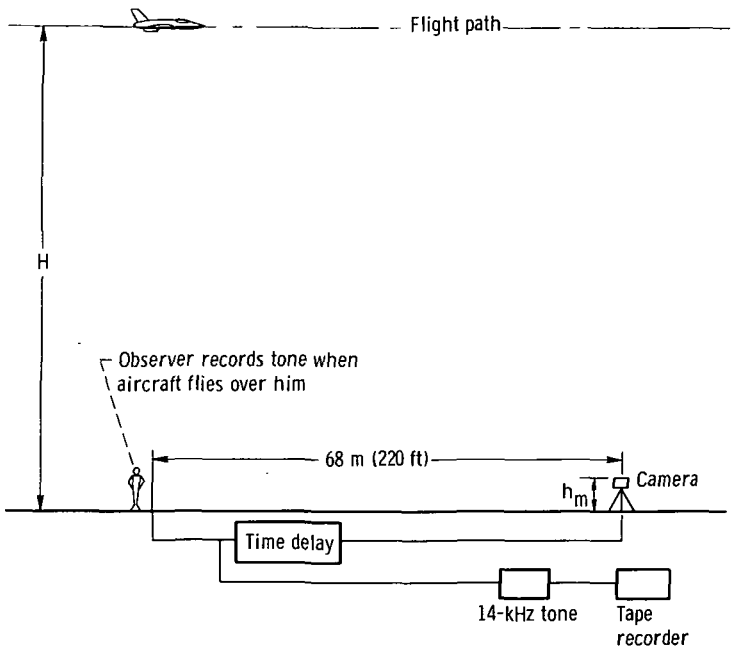

(a) Technique.

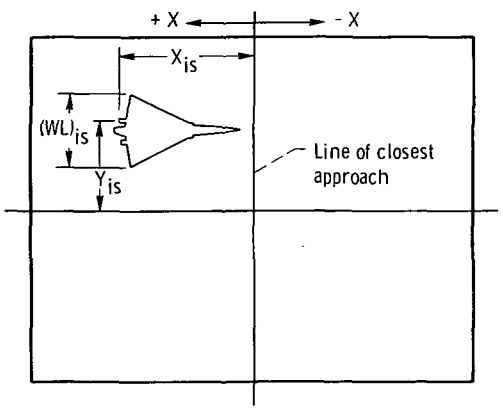

(b) Schematic of typical picture.

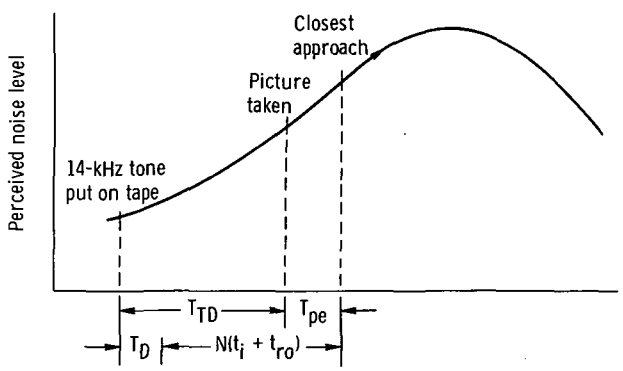

(c) Adjustment to time of closest approach.

Figure 26. - Determination of aircraft location.

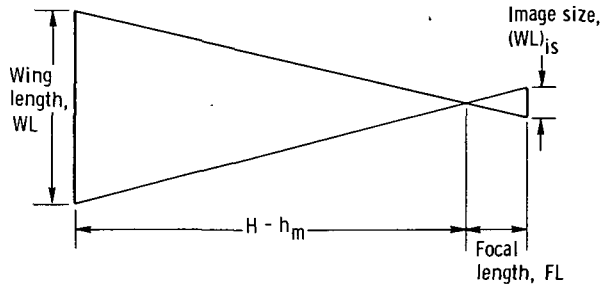

(d) Altitude determination.

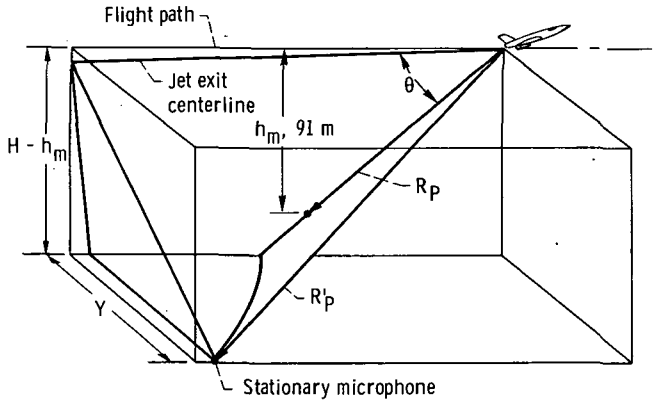

(e) Adjustment to 91-meter altitude directly beneath flight path.

Figure 26. - Concluded.

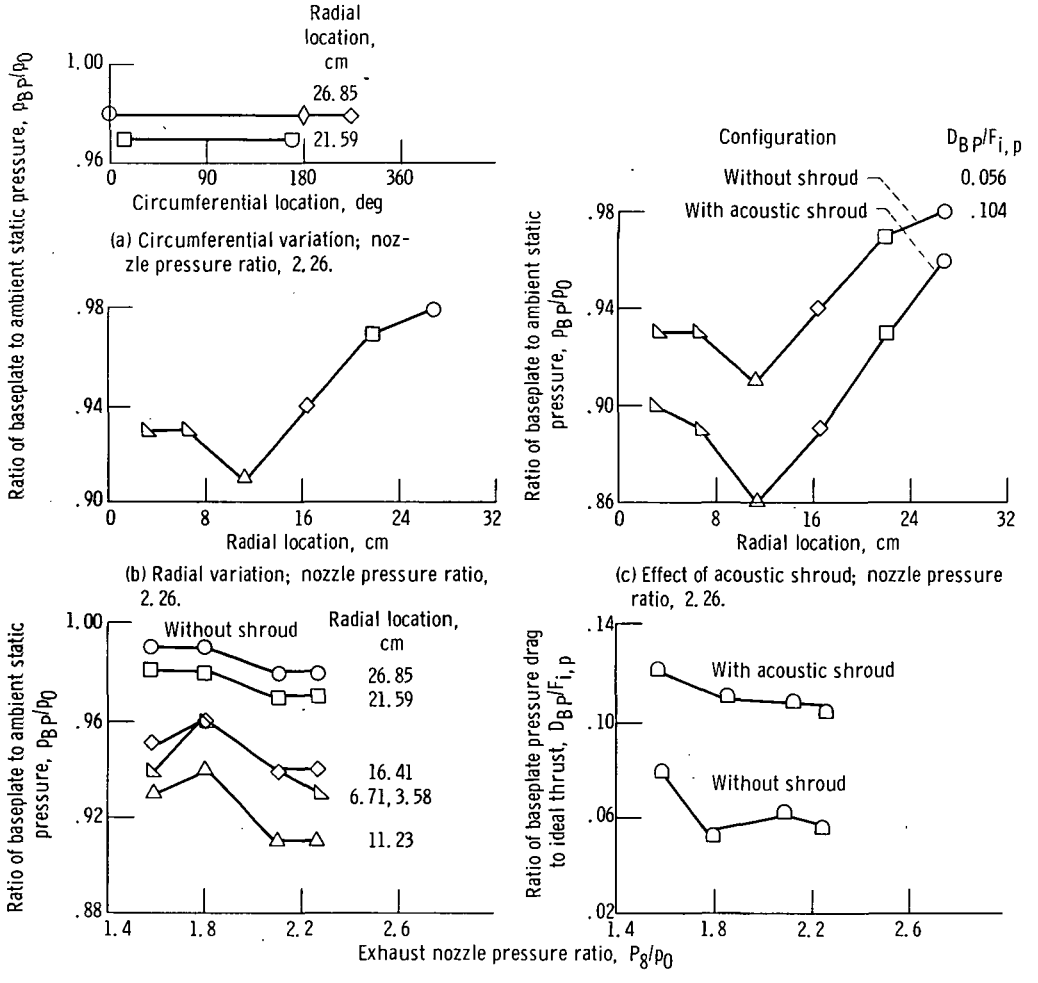

(a) Circumferential variation; nozzle pressure ratio, 2.26.

(b) Radial variation; nozzle pressure ratio, 2.26.

(c) Effect of acoustic shroud; nozzle pressure ratio, 2.26.

(d) Effect of nozzle pressure ratio.

Figure 27. - Baseplate pressures at static conditions.

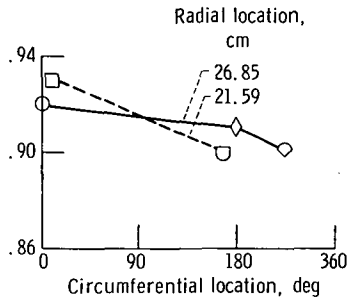

(a) Circumferential variation; nozzle pressure ratio, 2.53; corrected secondary weight flow ratio, 0.06.

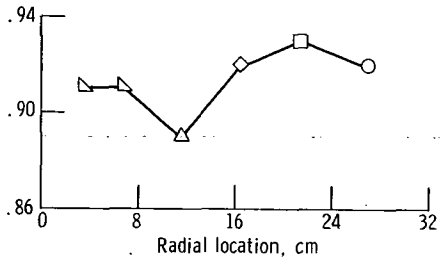

(b) Radial variation; nozzle pressure ratio, 2.53; corrected secondary weight flow ratio, 0.06.

Ratio of baseplate to ambient static pressure, p_{BP}/p_0

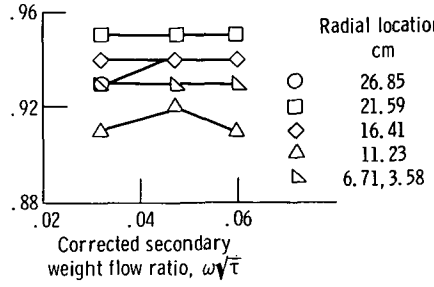

(c) Effect of corrected secondary weight flow ratio; nozzle pressure ratio, 2.53.

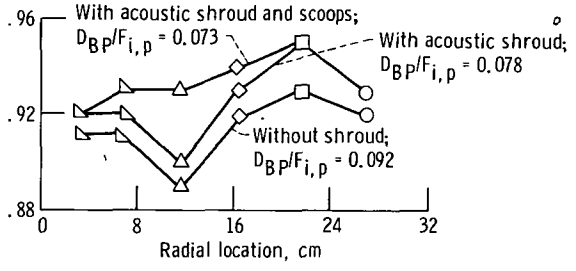

(d) Effect of acoustic shroud and scoops; nozzle pressure ratio, 2.53; corrected secondary weight flow ratio, 0.06.

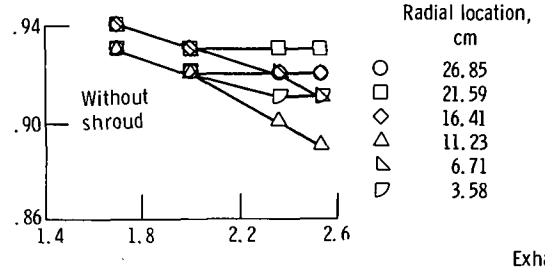

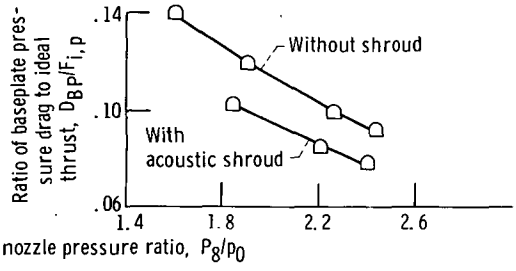

(e) Effect of nozzle pressure ratio; corrected secondary weight flow ratio, 0.06.

Figure 28. - Baseplate pressures at flyover conditions.

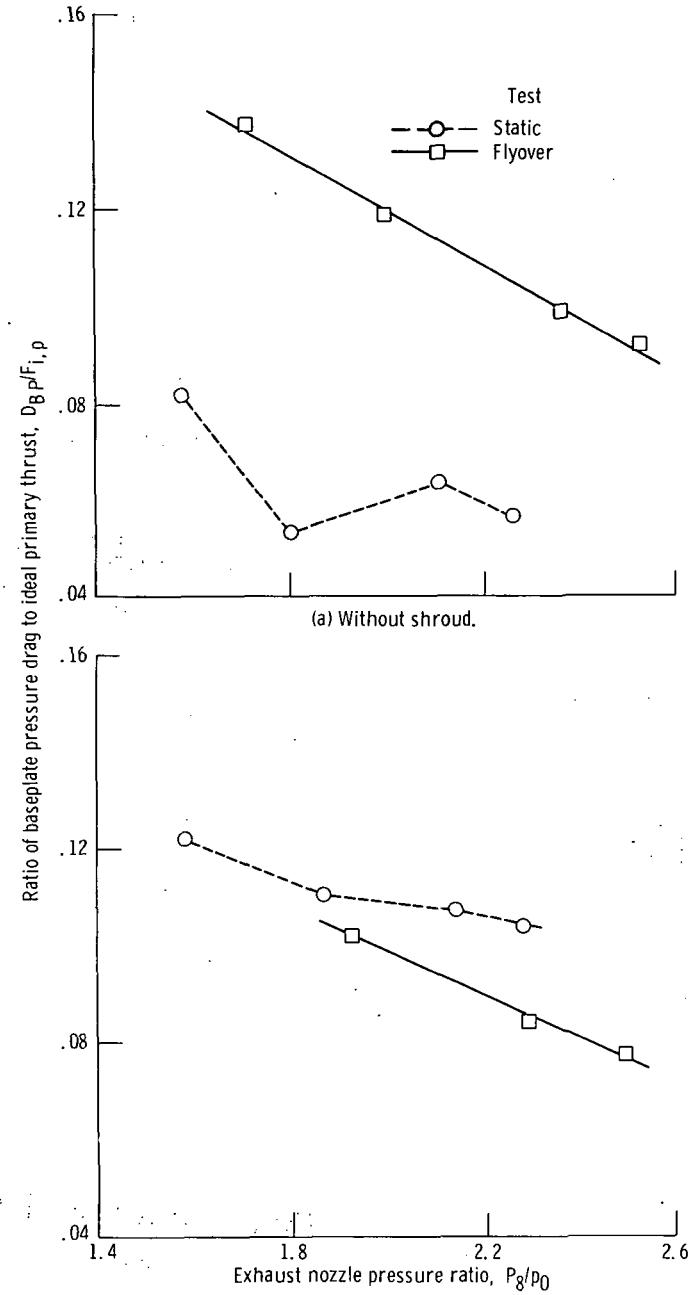

Figure 29. - Effect of flight velocity on ratio of baseplate pressure drag to ideal thrust.

Page Intentionally Left Blank

"The aeronautical and space activities of the United States shall be conducted so as to contribute . . . to the expansion of human knowledge of phenomena in the atmosphere and space. The Administration shall provide for the widest practicable and appropriate dissemination of information concerning its activities and the results thereof."

—NATIONAL AERONAUTICS AND SPACE ACT OF 1958

NASA SCIENTIFIC AND TECHNICAL PUBLICATIONS

TECHNICAL REPORTS: Scientific and technical information considered important, complete, and a lasting contribution to existing knowledge.

TECHNICAL NOTES: Information less broad in scope but nevertheless of importance as a contribution to existing knowledge.

TECHNICAL MEMORANDUMS: Information receiving limited distribution because of preliminary data, security classification, or other reasons. Also includes conference proceedings with either limited or unlimited distribution.

CONTRACTOR REPORTS: Scientific and technical information generated under a NASA contract or grant and considered an important contribution to existing knowledge.

TECHNICAL TRANSLATIONS: Information published in a foreign language considered to merit NASA distribution in English.

SPECIAL PUBLICATIONS: Information derived from or of value to NASA activities. Publications include final reports of major projects, monographs, data compilations, handbooks, sourcebooks, and special bibliographies.

TECHNOLOGY UTILIZATION PUBLICATIONS: Information on technology used by NASA that may be of particular interest in commercial and other non-aerospace applications. Publications include Tech Briefs, Technology Utilization Reports and Technology Surveys.

Details on the availability of these publications may be obtained from:

SCIENTIFIC AND TECHNICAL INFORMATION OFFICE

NATIONAL AERONAUTICS AND SPACE ADMINISTRATION

Washington, D.C. 20546